Magnetic resonance in iron-doped magnesium oxide

Vasquez Olano, Robinson A.

MAGNETIC RESONANCE

IN IRON-DOPED MAGNESIUM OXIDE

by

ROBINSON A. VASQUEZ OLANO, B.Sc.

A thesis submitted to the Faculty of Science of the University of Durham for the Degree of Master of Science

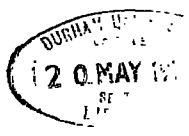

Department of Applied Physics
and Electronics
Science Laboratories
Durham City

March 1975

"VINI, VIDI, VINCI"

J. Ceaser

To the Memory of My Mother.

To My Father.

ACKNOWLEDGEMENTS

I should like to thank the British Council for the award of a scholarship which made possible the initiation of my studies, and to the Ford Foundation for economical support to complete these. Thanks are also given to the Department of Physics of the National University of Engineering of Lima, Peru, for encouragement and support through the development of my studies.

I am most grateful and indebted to Dr. J.S. Thorp, not only because of his constant guidance and dedication in supervising this research work, but also for his advice and help regarding my residence at the University of Durham.

My thanks are due to Professor D.A. Wright for allowing me to use the facilities of the Department, and to the technical staff led by Mr. F. Spence for their assistance. In particular, I am grateful to Mr. R. Waite for converting ideas into fine pieces of equipment.

I wish to thank Dr. C.A. Adcock who performed the theoretical calculation of the linewidth, and all the research students of the Ceramics and Resonance Research Group who, in one way or another, have contributed to the success of this research work. Among them Messrs. W. Hutton and E.A.E. Ammar deserve all my gratitude for their friendly willingness to help and advise in, as well as out of, the laboratories.

Last, but certainly not least, I would like to thank Mrs. J. Henderson who typed the manuscript of this thesis.

R.A. Vasquez
March, 1975

ABSTRACT

A linewidth analysis of the $\frac{1}{2} \leftrightarrow -\frac{1}{2}$ transition of Fe^{3+} in Magnesium Oxide crystals has been made using electron spin resonance techniques at x-band and at room and nitrogen temperatures. The values of linewidth at $\theta = 0^{o}$ (i.e. magnetic field along fourfold axis of the crystal) lay between 7 and 9 Gauss for specimens containing from 140 to 11900 p.p.m. Fe. The experimental linewidths measured for a range of samples show that the linewidth is concentration independent as opposed to the $(\text{concentration})^{\frac{1}{2}}$ dependence expected from Van Vleck's second moment theory. The discrepancy is explained on the grounds of exchange narrowing interaction between the ferric ions and the idea is supported by the values of the ratio of the fourth to second moments obtained by numerical integration of the absorption derivative line. The linewidth data indicates that the Fe^{3+} enters the lattice substitutionally, occupying Mg sites, at concentrations of up to 11,900 p.p.m. Fe. Preliminary spin-lattice relaxation time measurements have also been made using the pulse-saturation method at 35.5 GHz over the temperature range 4.2 - 27 K. Experimental evidence is presented for a fast relaxing process taking place in all the samples studied; this is explained in terms of spin exchange-interaction ($Fe^{3+} - Fe^{3+}$) by correlation with the proposed linewidth model. It also shows angular and concentration dependence and it is suggested that cross-relaxation between different parts of the spin system may account for variations observed. As regards the concentration dependence it is tentatively proposed that the spin-lattice relaxation time obeys a $(\text{concentration})^{-1}$ law and comparison is made with results published for other ions in the same host lattice. Using 9 GHz results available in the literature it is shown that Mattuck and Strandberg's $(\text{resonance frequency})^{-2}$ dependence for T_1 holds for Fe^{3+} in magnesia; furthermore there is approximate agreement of the experimental points with T^{-1} (direct) and T^{-7} (Raman) lines for the temperature variation which suggests that the slower relaxation process proceeds as for a single ion relaxing to the lattice.

CONTENTS

CHAPTER I

INTRODUCTION

Two topics of research recently undertaken in the Department have been based on industrial problems. These are related to the glass industry and to the electrical insulation industry respectively and can be summarized as follows.

In the glass industry, the transition element Titanium has been found to be an agent of nucleation in the crystallization of a wide variety of glasses including the low expansion Lithia-Alumina-Silica system, as well as the Magnesia-Alumina-Silica system, which is of importance due to its low dielectric loss characteristics. Empirical conditions have been established by the glass industry for the controlled crystallization of the aforementioned systems, although the mechanism by which the crystallization takes place is, as yet, uncertain. The research undertaken here concerns the role of Titanium in initiating crystallization and the primary technique employed is to include in the glass a paramagnetic monitor ion whose electron spin resonance behaviour may serve to indicate changes in local environment during crystallization. In the electrical insulators industry Magnesium Oxide, because of its insulating properties, has diverse applications; of these its use as an insulator in heating elements is being studied here. It has been found that at rather high temperatures ($\sim 800^{\circ}C$) the insulating behaviour of the MgO collapses and, consequently, the material conducts leadings to the failure of the element. It has been suggested that the diffusion of impurities from the shealth of the element, mainly iron, into the MgO lattice could be a possible explanation for the occurrence of such phenomenon; nonetheless, this argument has not been proved yet. In this study the main emphasis is to examine the electrical conductivity and dielectric losses in pure and doped Magnesia.

At first sight it might appear from the disparity between the aims of the two investigations and indeed from the techniques used that there is little connection between the two problems. Even though these differences exist a closer scrutiny reveals that in each case there is a noticeable common base of study: the Magnesium Oxide.

From the point of view of both researchers, particularly of the second, any additional information on the structure of the doped material, on the sites occupied by the dopant and on the magnetic behaviour of doping ions would be advantageous. This background provided the theme for the present work. The thesis reports on the study that has been carried out on iron doped Magnesium Oxide single crystals, using magnetic resonance as a tool. It was hoped that subsequently the data might bring more light towards an understanding of both of the above mentioned subjects of research.

Some electron spin resonance measurements on doped Magnesium Oxide have been reported and there are several papers dealing specifically with iron-doped Magnesium Oxide. However the emphasis of all these has been to determine the parameters of the Spin Hamiltonian, the g-factors, zero field splitting and so on. Indeed, almost all the transition elements have been studied in the MgO lattice using magnetic resonance as a technique, but the pattern of investigation is, without exception, that used for the iron doped Magnesia. In a recent work[1] on Neodymium-doped Calcium Tungstate, carried out in this Research Group, a rather different approach was adopted, viz. to correlate the E.S.R. linewidth with the predicted dipolar linewidth and so ascertain which atomic sites were occupied by the paramagnetic ion. In the present work this approach has been applied to iron-doped Magnesia and both experimental and predicted linewidth data are presented and compared. In addition some results are given for the spin-lattice relaxation behaviour of Fe in MgO in the temperature range 4.2 - 27 K.

CHAPTER II

GENERAL THEORY

This chapter, as the title suggests, is devoted to an outline of the basic theory which will be required to understand the experimental results obtained. It is by no means a complete and detailed account and it is advisable to consult the references quoted throughout the text if further information is desired. Two specific topics arise in this context; firstly, a few paragraphs describing the structure of Magnesium Oxide are given, and secondly the Hamiltonian, which is to be used to find out the energy levels of the ferric ion in the MgO lattice, is discussed.

II.1 THE MAGNESIUM OXIDE STRUCTURE

Magnesium Oxide crystallizes in the Sodium Chloride-like structure, as do almost a third of the compounds of the type MX, where M denotes a metal ion or atom and X an electronegative element, e.g. Oxygen, Fluorine, Chlorine, etc. In the case of MgO, M and X mean Magnesium and Oxygen respectively. Figure 2.1 provides an illustration of the MgO structure. The lattice is face-centred cubic with one atom associated with each lattice point, Mg at (0,0,0) and Oxygen at (0,0,½). Each of the two types of atom lies upon a face-centred cubic lattice, and each lies at the "largest interstice" of the other's f.c.c. lattice.

The largest interstice occurs at positions in the unit cell with co-ordinates (½,½,½) and equivalent positions (i.e. 0½0, 00½ and ½00). There are four of these per unit cell, hence one per lattice point; one largest interstice is illustrated in Figure 2.2. In fact, from Figure 2.2 it is clear that each atom has a co-ordination number of six, the neighbours being at the vertices of a regular octahedron.

In this octahedral co-ordination the ionic radii, according to Kelly and Groves[2], are of 0.65 Å for the Mg^{2+} and 1.40 Å for the O^{2-}. The lattice parameter of the MgO, at 21°C, is given by Wyckoff[3] as a_o = 4.2112 Å. In single crystals doped at low concentrations, such as the iron doped specimens used in the present experiment, it is generally assumed that the dopant enters the lattice substitutionally and that the average lattice parameter (or unit cell symmetry) is not changed.

II.2 THE CRYSTAL FIELD AND ZERO FIELD SPLITTING

By doping the MgO with iron, the latter is expected to go into the lattice by substitution of the magnesium sites. This assumption is based on the fact that the ferric ion (Fe^{3+}) has an ionic radius of 0.64 Å [2] which is almost the same as the corresponding ion Mg^{2+}. Although this assumption is fairly reasonable if one adopts the ionic radii as a point of comparison, there still remains to be considered the difference in electric charge between the trivalent doping ion and the divalent magnesium. The ferric ion with its five d electrons ($3d^5$) has a symmetrical charge distribution in its ground state but it is a poor fit in the magnesium oxide lattice because of the extra positive charge. Charge compensation in the crystal is effected either by excess oxigen ions[4] or by vacancies distributed at random throughout the crystal.

Considering then that the previous assumption is correct and bearing in mind Figure 2.2, it can be observed that the ferric ion will acquire an octahedral co-ordination and it is to be submitted to strong internal electric field exerted by the diamagnetic neighbours. In the main, the symmetry of this crystalline field will depend on the local arrangement of the diamagnetic ions rather than on the overall crystal

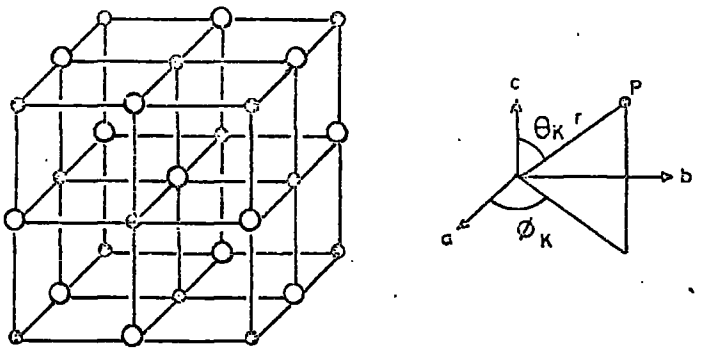

FIG 2·1. The Magnesium Oxide lattice

⊙ = Magnesium ○ = Oxygen

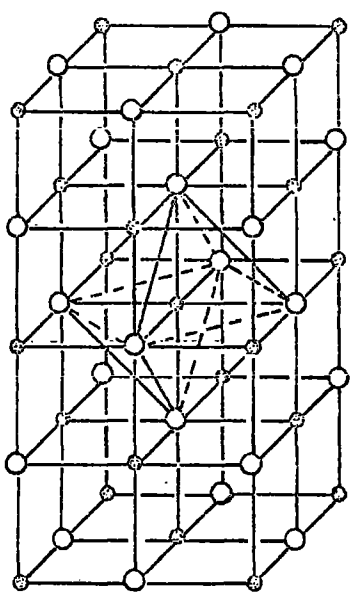

FIG 2·2. A Largest interstice in the MgO lattice

⊙ = Mg ○ = Oxygen

symmetry; the strength of the field being dependent on the distribution of the charges, on the amount of the charges of the various ions and on the distance of these charges from the paramagnetic ion. The action of this crystalline field is to shift and split the electronic energy levels. This splitting, in the absence of an external magnetic field, is known as "zero field splitting." The character of the splitting of energy levels of paramagnetic ions by the crystalline field depends to a great extent on the symmetry of this field. This circumstance enabled Bethe[5] to obtain a qualitative solution of the problem with the aid of group theory.

The ion Fe^{3+} has a ground state of $^6S_{5/2}$, and the resultant orbital momentum of the electrons equals zero. Through the spin-orbit interaction a crystalline field of cubic symmetry, as it will approximately result from the octahedral arrangement of the six oxygens surrounding each paramagnetic ion, splits the sixfold degeneracy into a twofold degenerate level and a fourfold degenerate level[5]. Van Vleck and Penney[6] have discussed the mechanism by which such a splitting can be effected and have shown that the crystalline cubic field can influence the electron spins only through high order interactions involving spin-orbit coupling with excited states. When the spin-orbit coupling interaction is much less than the crystal field splitting, the wave function of the ground crystal field state will contain admixtures of the next higher state, and as a result of this admixture the g-factor of a transition-metal ion deviates from its free electron value by a term that is proportional to the spin-orbit coupling constant and inversely proportional to the crystal field splitting. For the ferric ion in the Magnesium Oxide lattice, Low[7] has found the zero field splitting to be $3a = 615 \times 10^{-4}$ cm^{-1}; this value corresponds to a magnetic field of 658 Gauss[8]. Figure 2.3 shows a diagram of the zero field splitting of the $^6S_{5/2}$ state in a cubic field.

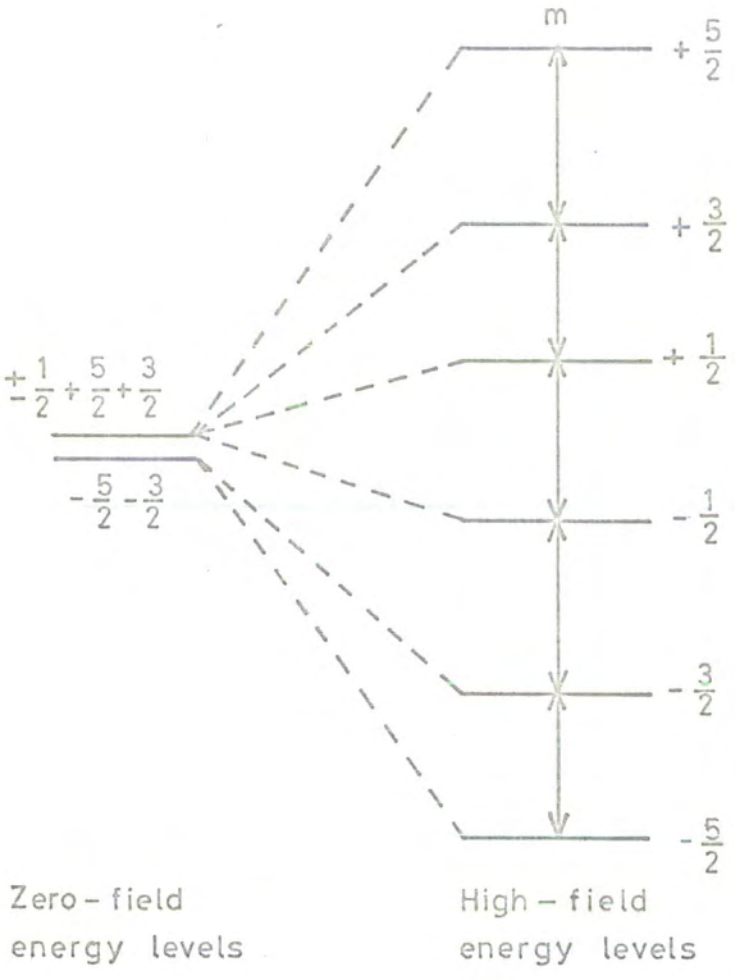

FIG 2·3. Energy levels of the $^6S\,\frac{5}{2}$ state in a cubic field with zero field splitting of $3a = 658$ Gauss.

II.3 THE SPIN HAMILTONIAN AND ENERGY LEVELS

The energy of an atom or radical containing unpaired electrons and nuclei with non-zero spins may be expressed in terms of the Hamiltonian operator[9]:

$$H = H_{e\ell} + H_{CF} + H_{LS} + H_{SS} + H_{Ze} + H_{Zn} + H_{II} + H_{Q}$$

where the first three terms constitute the atomic Hamiltonian and the last six form the spin Hamiltonian. The operator $H_{e\ell}$ accounts for the electronic kinetic and potential energy as well as for the interelectronic repulsion. It is many orders of magnitude larger than the Zeeman energies (10^4 - 10^5 cm^{-1}), therefore it is in the optical region of the spectra. The crystalline field H_{CF} operator has the general form of

$$H_{CF} = \sum_i - eV\ (x_i, y_i, z_i)$$

where V is the potential of the crystalline field and x_i, y_i, z_i are the co-ordinates of the i-th electron of the unfilled shell. In the very particular case in which the polar z-axis coincides with a fourfold axis of symmetry the potential V adopts the form[10]

$$V_{cub} = C_4 \left(x^4+y^4+z^4-\frac{3}{5} r^4 \right) + \ldots.$$

where C_4 is a parameter which depends on the symmetry of the arrangement of charges which create the crystalline field. V_{cub} expressed in operator equivalent is written as

$$\frac{1}{6} a \left[S_x^4 + S_y^4 + S_z^4 - \frac{1}{5} S(S+1)\ (3S^2+3S-1) \right]$$

where S_x, S_y, S_z are the projections of the operator spin along the axis of the frame of reference.

The crystalline field energies are of many thousands of cm^{-1} (for the first transition series, i.e. $3d^n$ configuration) and far exceed the electronic Zeeman interaction of about 0.3 cm^{-1}; hence they are

directly detected in optical spectroscopy. However, they strongly influence the magnitude and anisotropy of the spin Hamiltonian parameters.

The spin-orbit H_{LS} operator is frequently written as

$$H_{LS} = \lambda \bar{L}.\bar{S}$$

whereas a general expression for the spin-spin H_{SS} operator is given by

$$H_{SS} = -\rho \left[(\bar{L}.\bar{S})^2 + \frac{1}{2} (\bar{L}.\bar{S}) - \frac{1}{3} L (L+1) S (S+1) \right]$$

The spin-orbit energies (10^2 cm^{-1}) are much smaller than typical crystal field splittings for the first transition series. The spin-spin energies (0 - 10 cm^{-1}) are frequently of the same order of magnitude as the electronic Zeeman energies, in which case the spectrum becomes strongly angular dependent. The Zeeman H_{Ze} energy is expressed by means of the well known form

$$H_{Ze} = g \beta \bar{H}.\bar{S}$$

and has the value of approximately 0.3 cm^{-1} at X band and is sometimes anisotropic. The hyperfine H_{HF} operator takes the form

$$H_{HF} = A \bar{S}.\bar{I}$$

and the Zeeman nuclear H_{Zn} term

$$H_{Zn} = -\gamma \beta_N \bar{H}.\bar{I}$$

The nuclear spin-spin interaction has the same form as the hyperfine operator

$$H_{II} = J \bar{I}.\bar{I}$$

So far the different contributions that are possible to take into account in the Hamiltonian corresponding to a very general system have been briefly mentioned. Fortunately in the case of the ferric ion

in the Magnesium Oxide lattice it is possible to omit most of the terms either due to their very small contribution to the total Hamiltonian or to the fact that they are equal to zero. For instance, since the resultant angular momentum of the ion is zero (S ground state) evidently $H_{LS} = 0$; moreover, no hyperfine structure is expected since the ion has an S ground state[11,12]. The Fe^{3+} ions in MgO are found to occur almost entirely in a pure cubic field[13] therefore the cubic form of the H_{CF} operator is applicable. Summing up all these simplifications, Low[14] writes as a Hamiltonian for the ferric ion in the Magnesium Oxide lattice:

$$H = g\beta \bar{H}.\bar{S} + \frac{1}{6} a \left[S_x^4 + S_y^4 + S_z^4 - \frac{1}{5} S(S+1)(3S^2+3S-1)\right]$$

where the first term represents the splitting caused by the action of the external field H on the various spin levels and the second one accounts for the zero field interaction. The energy levels of the $^6S_{5/2}$ state have been calculated by Debye[15] and by Kronig and Bouwkamp[16]. To the second order in perturbation theory, the energy levels in a strong magnetic field with direction cosines (ℓ,m,n) with respect to the fourfold axis are[17]:

$$\pm\frac{5}{2}: \qquad \pm\frac{5}{2} g\beta H + \frac{1}{2} pa \pm (212-24p-113p^2)(a^2/240\, g\beta H)$$

$$\pm\frac{3}{2}: \qquad \pm\frac{3}{2} g\beta H - \frac{3}{2} pa \pm (12 + 8p - 15p^2)(a^2/16\, g\beta H)$$

$$\pm\frac{1}{2}: \qquad \pm\frac{1}{2} g\beta H + pa \pm (-2 - 3p + 5p^2)(a^2/3\, g\beta B)$$

where $p = 1 - (\ell^2m^2 + m^2n^2 + n^2\ell^2)$.

The transitions, their positions and their relative intensities are given as follows:

TRANSITION	POSITION	REL. INT.
$\frac{5}{2} \leftrightarrow \frac{3}{2}$	$h\nu = g\beta H + 2pa + (2-9p+7p^2)(a^2/15g\beta H)$	5
$\frac{3}{2} \leftrightarrow \frac{1}{2}$	$= g\beta H - \frac{5}{2} pa + (68+72p-125p^2)(a^2/48g\beta H)$	8
$\frac{1}{2} \leftrightarrow -\frac{1}{2}$	$= g\beta H + (-2-3p+5p^2)(2a^2/3g\beta h)$	9
$-\frac{1}{2} \leftrightarrow -\frac{3}{2}$	$= g\beta H + \frac{5}{2} pa + (68+72p-125p^2)(a^2/48g\beta H)$	8
$-\frac{3}{2} \leftrightarrow -\frac{5}{2}$	$= g\beta H - 2pa + (2-9p+7p^2)(a^2/15g\beta H)$	5

In sufficiently strong fields, where terms of order $a^2/g\beta H$ can be neglected, the resonance spectrum consists just of five lines for which $\Delta m = \pm 1$. Their relative intensities follow from the square of the matrix elements, which is just $S(S+1) - m(m-1)$ for the transition $m \leftrightarrow (m-1)$. The lines form a symmetrical pattern as shown in Figure 2.4.

Considering next the angular dependence it is found that the spectrum retains the same form for all directions of the magnetic field, but with varying displacement of the outer lines depending on the quantity p. This displacement varies with angle in the same way as the cubic potential, since p can be written in the form[17]:

$$2p/5 = \ell^4 + m^4 + n^4 - 3/5$$

The extreme values of p are:

$p = 1$ along the <100> -axis ,

$p = -2/3$ along the <111> -axis ,

$p = -\frac{1}{4}$ along the <011> -axis .

In the first case (p = +1, i.e. H field in <100> -axis) and using the strong magnetic field approximation ($\beta H >> a$) the transitions are given approximately as:

$$-\frac{1}{2} \leftrightarrow -\frac{3}{2} \qquad h\nu = g\beta H + \frac{5}{2}a$$

$$\frac{5}{2} \leftrightarrow \frac{3}{2} \qquad = g\beta H + 2a$$

$$+\frac{1}{2} \leftrightarrow -\frac{1}{2} \qquad = g\beta H$$

$$-\frac{3}{2} \leftrightarrow -\frac{5}{2} \qquad = g\beta H - 2a$$

$$\frac{3}{2} \leftrightarrow \frac{1}{2} \qquad = g\beta H - \frac{5}{2}a$$

At X band (9.100 GHz), and taking the accepted value of g = 2.0037, the expected positions of the lines for the case in which the external magnetic field H is applied along the fourfold axis of the crystals, are summarized in Table I.

TABLE I

Predicted spectrum of the MgO : Fe^{3+} at 9.100 GHz and H//<100> -axis

Transition	$-\frac{1}{2} \leftrightarrow \frac{3}{2}$	$\frac{5}{2} \leftrightarrow \frac{3}{2}$	$+\frac{1}{2} \leftrightarrow -\frac{1}{2}$	$-\frac{3}{2} \leftrightarrow -\frac{5}{2}$	$\frac{3}{2} \leftrightarrow \frac{1}{2}$
H_{res} (Gauss)	2697	2807	3245	3683	3793
Rel. Inten.	8	5	9	5	8

The energy level diagram showing the expected transitions in the 3 centimeter region is presented in Figure 2.5. The diagram has been drawn for the case in which the H field is along the fourfold axis. No energy level diagrams appear to have been published for other polar angles, however W. Low[7] reported that the $+1/2 \leftrightarrow -1/2$ transition is isotropic.

The theory concerning linewidth and spin-lattice relaxation time measurements is given in Chapters IV and V respectively, together with the experimental results.

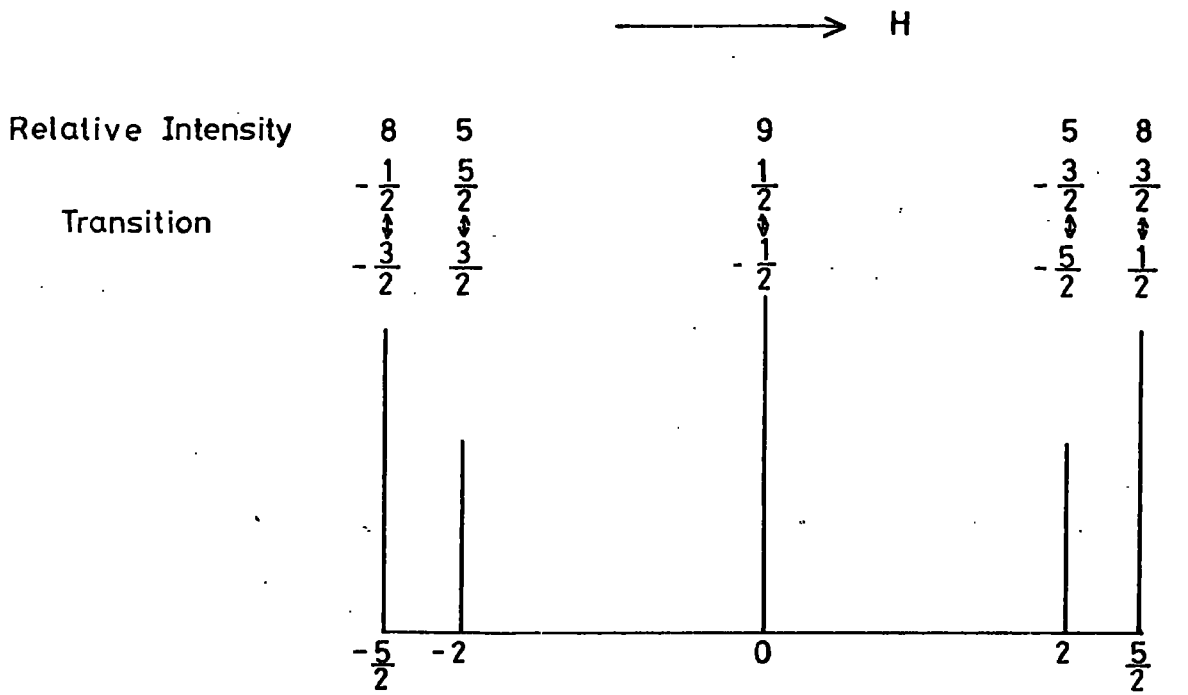

FIG 2·4 SPECTRUM FOR S = $^{5}/_{2}$, CUBIC FIELD SPLITTING, IN STRONG MAGNETIC FIELD.

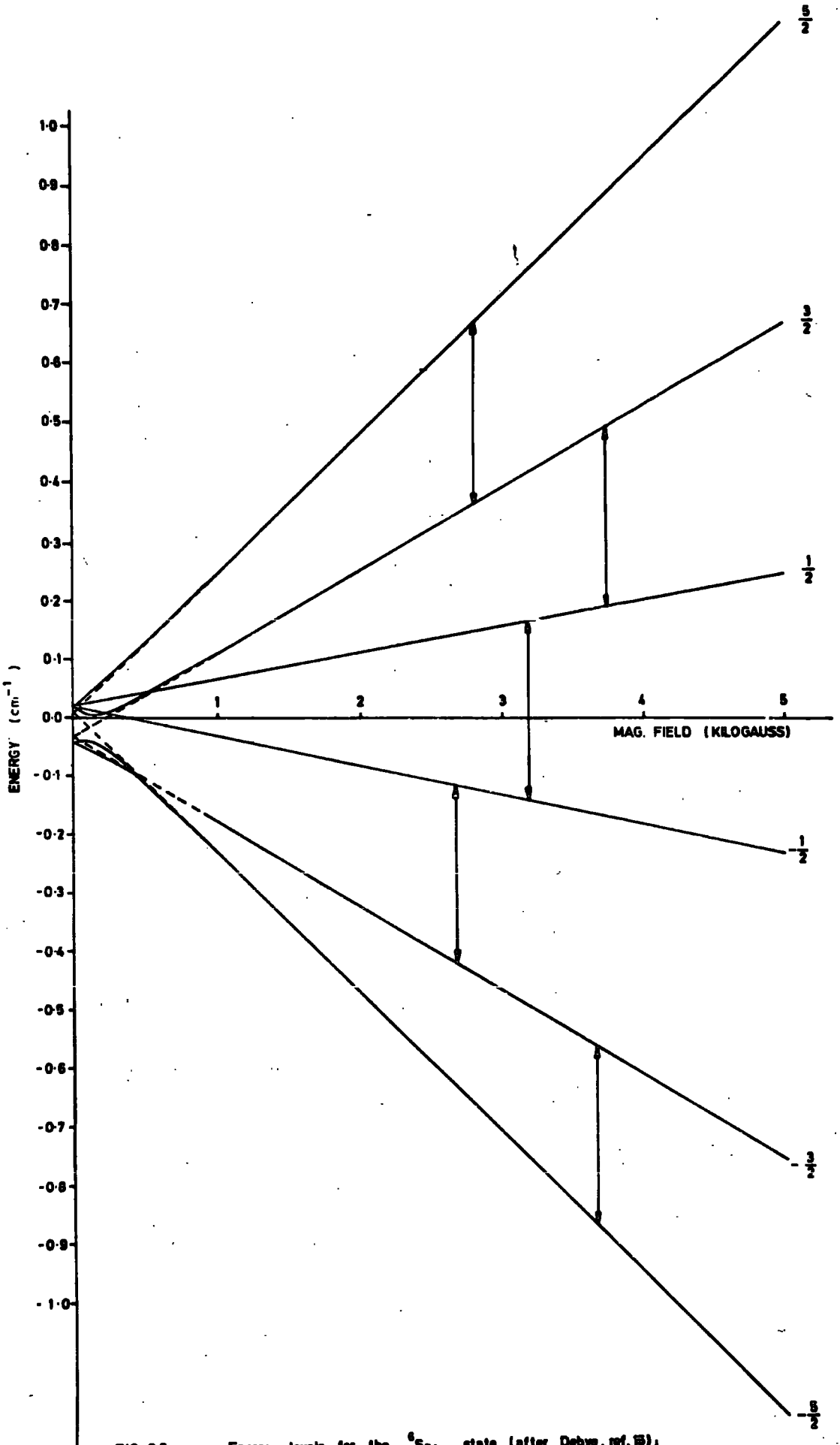

FIG. 2·5 Energy levels for the $^6S_{5/2}$ state, (after Debye, ref. 15); H along fourfold axis of the crystal; transitions shown for a frequency of 9·100 GHz.

CHAPTER III

EXPERIMENTAL TECHNIQUES

Once the line of work had been determined, it remained to be decided whether to obtain the experimental data at Q band or at X band; that is, at frequencies of 35.5 GHz or 9 GHz respectively. The advantage of the first option was the availability of a spectrometer operating at this frequency and provided with all the necessary facilities to perform experiments at liquid nitrogen and liquid helium temperatures which eventually might have been considered necessary to execute; whilst the advantage of the second alternative was the existence of many publications on E.S.R. in the 3 centimeter region and in particular those dealing with the subject of interest of this thesis, i.e. doped Mangesium Oxide. On balance it was thought wise to work at X band since the previous information could be used as a means for checking the progress during the initial stages of obtaining experimental data. This course was therefore adopted, even though it involved the need to build up an X-band spectrometer, since there was not one at hand in the Department's laboratories. The first task, therefore, was to construct a 3 cm spectrometer which could subsequently be used to get E.S.R, data from the MgO samples and also from a range of materials likely to be investigated a posteriori. To this end the remains of an old non-operational unit were used to make a virtually new system, and a brief account of the results achieved are given here.

III.1 THE X-BAND SPECTROMETER AND LINEWIDTH MEASUREMENTS

Two basic types of spectrometers are of widespread use. In the first type the paramagnetic resonance absorption is detected by the change in the power transmitted through the cavity resonator containing

the sample, and in the second the absorption is detected by the change in power reflected from the cavity. There are common features since in any case, every microwave spectrometer consists of the following basic parts: a microwave source, a means of storing energy in the form of a cavity resonator, a detector, an amplifier and recording device, and a source of steady magnetic field. In the majority of cases we must add to these parts a system for modulation of the steady magnetic field which together with a phase sensitive detection enables one to obtain derivative outputs and correspondingly greater sensitivities. To this extent, the setting up of the spectrometer constructed did not differ from that of any conventional one of its type and the basic principle of operation of the equipment could be explained in exactly the same way as all the reflection spectrometers, i.e. the variation of the Q-factor of a resonant system[18].

The microwave power, which is to excite the electronic transitions, is provided by a type KS9 - 20A Mullard klystron. A magic T splits this power equally into two of the arms of a bridge, one of which includes an attenuator and a phase-shifter (for intially balancing the system in phase and amplitude), whilst the other leads to the resonant cavity which contains the crystal under study. At the extreme of the third arm a diode is placed as a detector of the output of the balanced bridge, that is the crystal output was proportional to the absorption by the sample at resonance, and, additionally, a high-Q wavemeter to measure the operating frequency is connected also.

The rectangular resonant cavity is made of silver plated brass (to increase the Q-factor) and has dimensions 2.27 cms x 1.01 cms x 3.58 cms. It works in the TE_{102} mode and it is iris-coupled to a Cu/Ni waveguide. A diagram of the cavity is shown in Figure 3.1a

which shows the selected location of the sample also. Figure 3.1b shows the matching device as it was in the early style. It consisted of a brass screw capable of moving in and out of the waveguide perpendicular to its broad face. It was found that putting the sample inside the cavity altered the resonance frequency and the matching conditions by amounts depending on crystal size and doping. At room temperature the use of the brass screw was good enough to obtain cavity resonance conditions and acceptable matching, i.e. to pre-set the cavity system before magnetic resonance measurements were made; but at the time when a low temperature experiment was to be done the above mentioned method failed to work as there was no access to the screw due to the presence of a double Dewar set surrounding the cavity. To overcome this inconvenience, a continuously adjustable system for low temperature operation was designed and built (with the help of W. Hutton) in such a way that the samples could now be matched by remote control from outside the cryostat. A scheme of this dispositive is illustrated in Figure 3.2.

The source of the necessary steady magnetic field is an electromagnet, which is capable of being rotated to enable polar plots to be made. Using the technique of proton resonance measurement, it was found that the homogeneity of the field is of few parts in 10^3 over a volume of one cubic centimeter, i.e. it is sufficiently uniform over a volume greater than that of the sample. The rate of change of the field is controlled by means of a sweep unit which drives the power supply of the magnet, the minimum rate employed being five gauss per second. The magnet is also provided with two Helmholtz coils attached to the pole pieces, which connected to a radiofrequency oscillator, will in turn sweep the magnetic field. This method of field modulation is, as it is well known, to increase the overall sensitivity of the spectrometer[19].

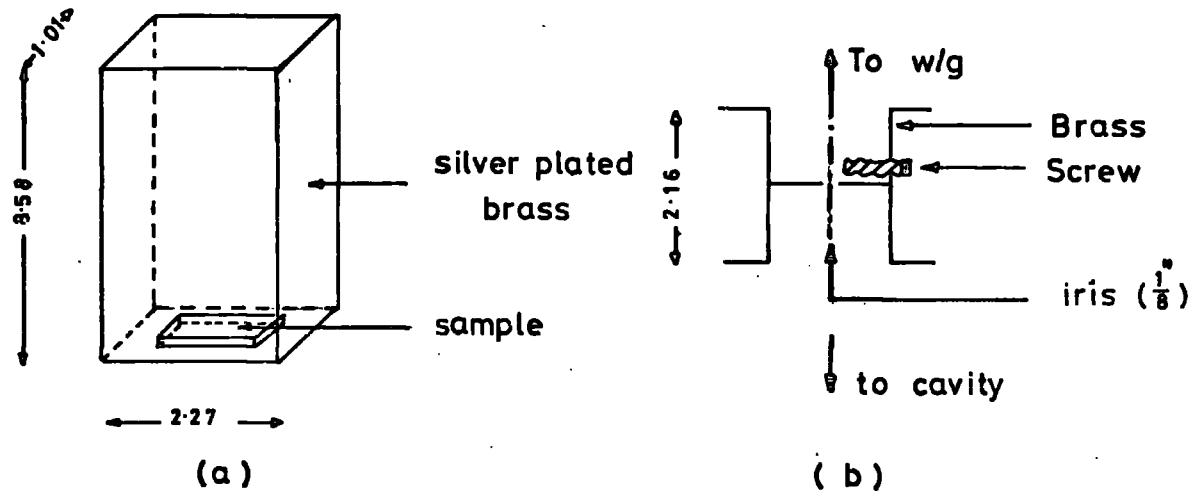

FIG 3·1. (a) Cavity showing sample position, (b) Matching device (early style). Dimensions in cms.

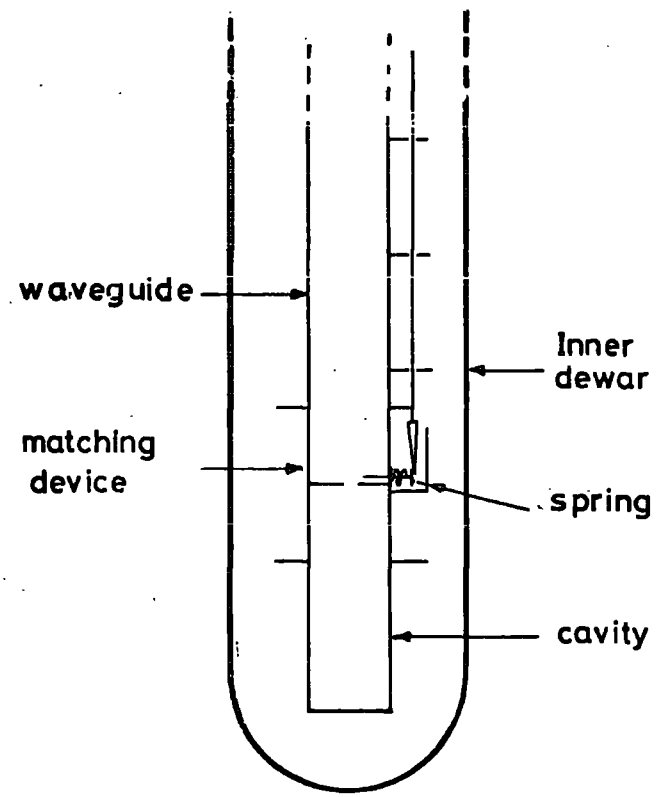

FIG 3·2. Continuosly adjustable matching device for 77 K measurements.

An arrangement of a phase sensitive detector, a phase shifter and a low-noise amplifier tuned at the modulation frequency (125 Hz in this case) completed the system used to "process" the signal from the detector output. The y-axis of a pen recorder is fed with the output of the phase sensitive detector, whilst the x-axis is connected to the output of the sweep unit so that a plot of the derivative of the resonance line versus magnetic field is obtained. In Figure 3.3 a block diagram of the spectrometer is presented, showing the cryogenic facilities that were added to enable measurements at low temperatures. As the sensitivity of an E.S.R. spectrometer is proportional to the ratio of the signal amplitude to the noise amplitude on a recorder display, a standard ruby crystal was used to find out this value giving as a result 1.7×10^{15} spins/ΔH as an overall sensitivity for the X-band spectrometer at room temperature.

In order to measure the linewidth, the whole spectrum was recorded by scanning the main magnetic field over a 1 Kilogauss wide range and from there the transitions were identified. To ensure better accuracy in the measurement the rate of scan of the magnetic field through the selected transition was reduced down to usually 100 Gauss in 32 seconds (about 4 Gauss per second). The modulating radiofrequency field was kept at a level such that no artifical broadening of the line due to saturation effect was observed. This level was determined experimentally.

Both the initial and the final points of the magnetic field scanned were measured using proton resonance and it was assumed that the sweep was linear in the region under consideration. False measurements due to hysteresis problems were avoided by sweeping repetitively the magnetic field up and down the same region before any reading was taken. From the calibrated scale, linewidths were measured as the separation, in units of magnetic field, of the two turning points of the derivative curve.

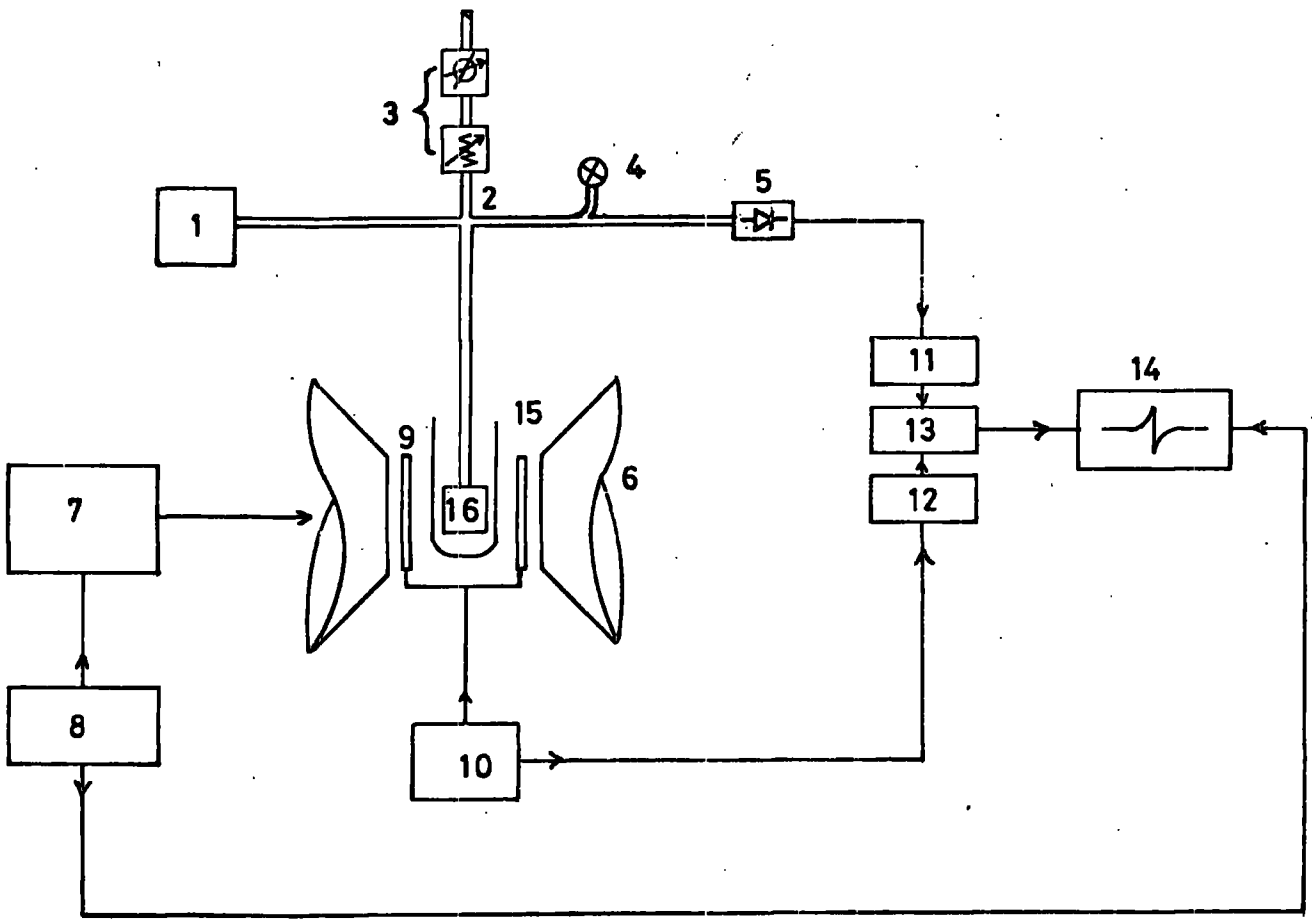

1 Klystron
2 Magic T
3 Attenuators
4 Wavemeter
5 Detector
6 Magnet
7 D.C. Power Supply
8 Sweep Unit
9 Modulation Coils
10 Audio-frequency Oscillator
11 Low Noise Amplifier
12 Phase Shifter
13 Phase Sensitive Detector
14 Recorder
15 Cryogenics for 77 K
16 Cavity

FIG. 3·3 Block diagram of the X-band E.S.R. Spectrometer.

III.2 Q-BAND SPECTROMETER AND T_1 MEASUREMENTS

With the aid of the X-band spectrometer it was possible to obtain all the necessary data as far as linewidth measurements were concerned; however, it could not be used to obtain spin-lattice relaxation time data because of the lack of facilities to perform this type of experiment.

As has been mentioned in previous paragraphs, there existed in the Department's laboratories a Q-band spectrometer which had been designed in such a way that spin-lattice relaxation time measurements could be made by the pulse saturation method. As G. Brown et al[20] had described the spectrometer which has been used in the present work, a detailed description will be omitted here. Nonetheless, it is perhaps worthwhile to remark that although the spectrometer resembles a typical one of its type there is, however, a substantial difference: the samples are located inside a section of waveguide and a plunger short-circuits the latter, as opposed to the use of a resonant cavity which is the most common device used to store electromagnetic energy. The absence of a cavity means, of course, a low Q-factor ($\sim$ 400) but in the end it turns out to be advantageous as it is easier for the setting of the two klystrons which are to be used in T_1 measurements.

The use of transient techniques in magnetic resonance has been more widely exploited in the field of Nuclear Magnetic Resonance than in Electron Spin Resonance, and the major part of the basic theory was formulated with reference to NMR research. Woonton[21] has reviewed E.S.R. pulse techniques as well as some other researchers, such as Pace et al[22]. In essence, the pulse method consists in (1) exposing the sample to a very high power, short-duration pulse of microwave energy, and (2) measuring the strength and decay rate of the induced magnetization. Figure 3.4 shows schematically this situation. Davis et al[3] emphasized that the saturation method of determining E.S.R. relaxation

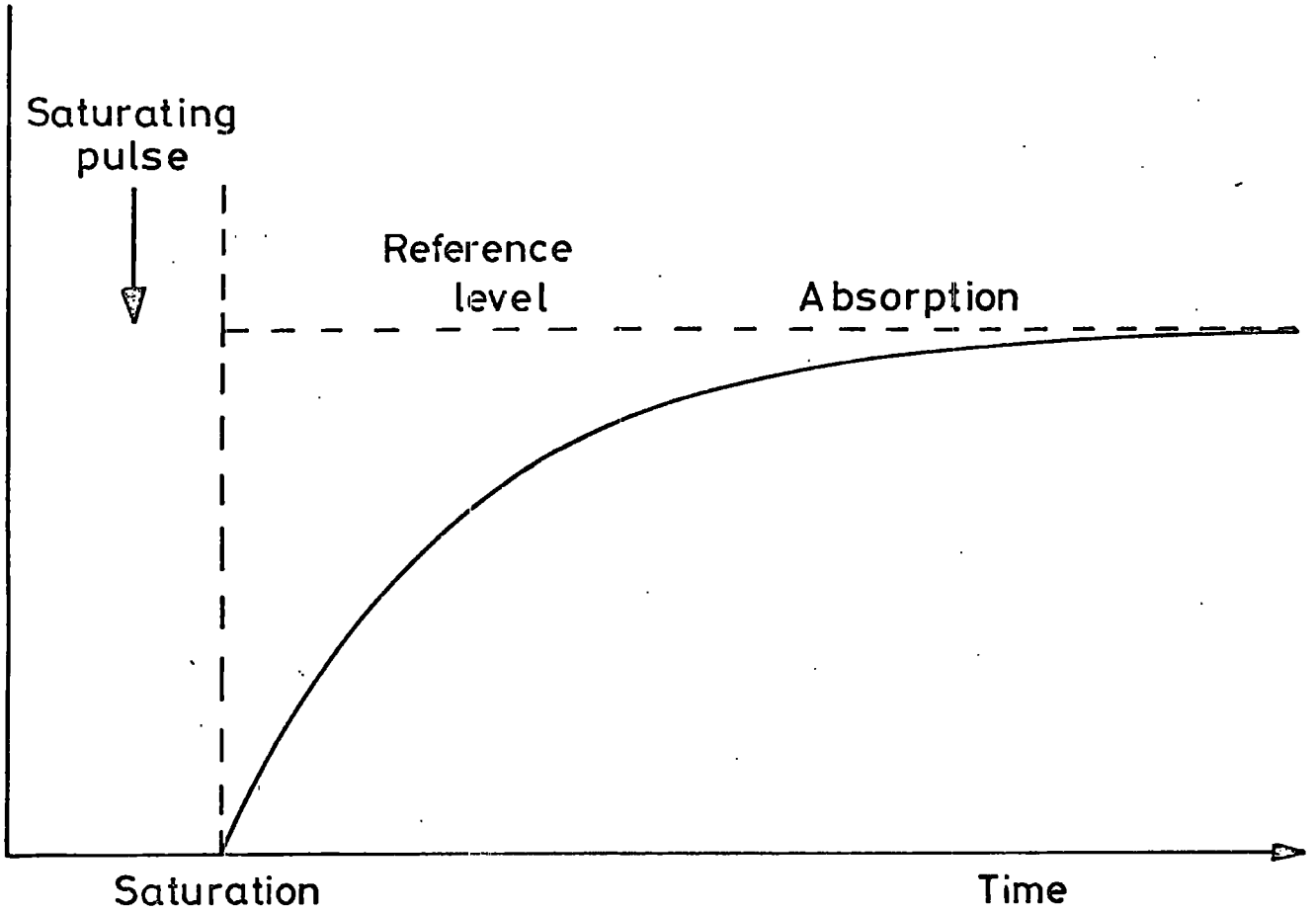

FIG 3·4. Sequence of operations in the pulse saturation technique.

times employs "continuous wave (CW) techniques in the frequency domain", and that the interpretation of such data depends upon the assumption of a physical model such as the Bloch theory.

In practice, a low power microwave energy was applied to the sample by a 20 milliwatt reflex klystron and the external magnetic field was set up at the peak of the absorption line so that maximum D.C. level could be obtained from the output of the amplifier. This maximum D.C. level was fed to the y-axis of an oscilloscope. In this condition, a 20 Watts pulse, 30 milliseconds long and with a repetition rate of 10 cycles per second was superimposed on to the CW low power microwave energy and as a result the characteristic exponential decay appeared displayed in the oscilloscope. The recording of this curve was made using Polaroid film and for this purpose the repetition rate of the high-power pulse was reduced to one cycle per second in order to obtain a single shot situation. A typical photograph which was obtained from the oscilloscope is shown in Figure 3.5. From the photographs, the amplitude of the signal was measured and the natural logarithm of it as a function of time was plotted to check for single exponential decay. The best straight line was fitted to the experimental points using the method of Least Squares and a computing program was written for this purpose. From the slope of this line the spin-lattice relaxation time was obtained as a final figure.

Spin-lattice relaxation times were measured in the temperature range of 4.2 K up to 25 K, by letting the system warm up at controlled rates using a device designed and constructed by W. Hutton and E.A.E. Ammar, which essentially consisted of a large block of a special araldite[24], which had a large thermal capacity, surrounding the specimen and waveguide assembly.

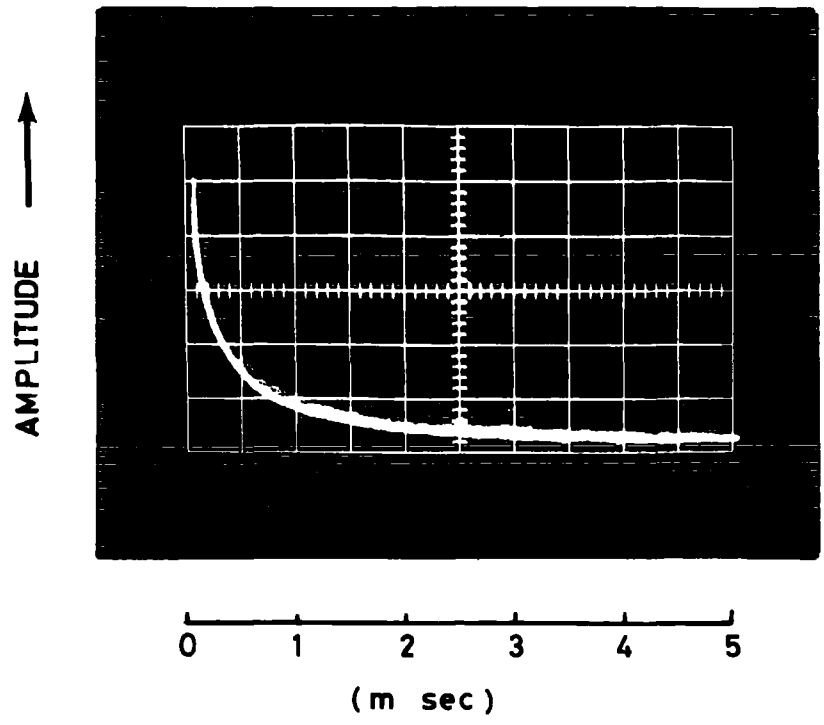

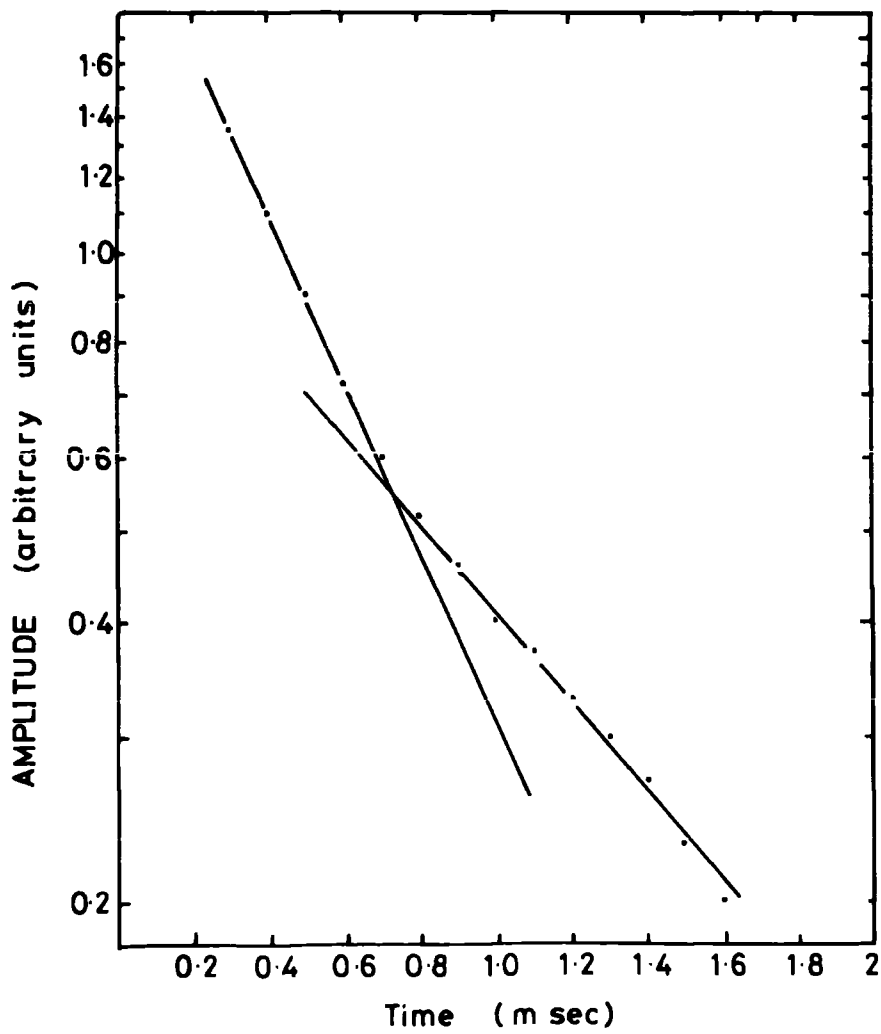

FIG. 3·5. (a) Typical Exponential decay photograph, (b) Semilogarithmic plot to determine T_1

III.3 THE IRON-DOPED MAGNESIA SAMPLES

The iron-doped Magnesium Oxide single crystals used in the present work were obtained from W. & C. Spicer Ltd., Cheltenham, and were grown by electrofusion from powder. They were analized by optical spectrographic techniques and their orientation finally checked using the X-ray back reflection method of Laue.

The concentrations available were:

Reference No.	1	2	3	4	5	6	7	8
Concentrations	140	310	710	2300	4300	8500	11900	12900

where the concentrations are given in parts per million of iron. The material was in good single crystal form. To the eye, even at the higher concentrations, the crystals appeared to be free from cracks or inclusions: they were transparent and coloured from light yellow-green to dark yellow-green according to iron concentration. The X-ray back reflection photographs confirmed the single crystal nature of the specimens: the diffraction spots were sharp and there was not indication of strain or mosaic formation. All crystals were cut to the dimensions 9.8 mm x 7 mm x 2.6 mm in order to fit the Q-band waveguide as well as the optical spectrometer holder.

CHAPTER IV

LINEWIDTH MEASUREMENTS

A great deal of information can be obtained from a careful analysis of the width and shape of a resonance absorption line. It is a powerful tool for studying the relaxation and exchange mechanisms connected with the magnetization process and, for the purpose of the present work, enables one to ascertain which atomic sites are occupied by the dopant in the MgO lattice by correlation of the experimental linewidths with the theoretical expected value.

IV.1 GENERAL THEORY

There are two principal types of resonant lines in solids, those that are homogeneously broadened, and those that are inhomogeneously broadened. The former are pure spectral singlets whereas the latter type consists of a spectral distribution of much narrower homogeneously broadened lines.

Homogeneous broadening occurs when the magnetic resonance signal results from a transition between two spin levels which are not sharply defined, but instead, are somewhat intrinsically broadened. Several sources of homogeneous broadening are[25]:

(i) Dipolar interaction between like spins

(ii) Spin-lattice interaction

(iii) Diffusion of excitation throughout the sample

(iv) Motional narrowing fluctuations in the local field .

If two neighbouring paramagnetic centres are located at a distance r from one another, each Zeeman energy level is broadened by the value $\sim h/\beta^2 r^{-3}$ as a result of the dipole interaction. This may be intuitively

visualized as follows: Besides the external magnetic field H_o, a local field H_{loc} created by the neighbouring particles also acts on each paramagnetic centre; the resonance condition therefore takes the form $h\nu = g\beta(H_o + H_{loc})$, and since the mean spread values of H_{loc} is of the order of β/r^3, a spread in the resonance condition results of the order of magnitude which has been mentioned above. If all paramagnetic particles are identical then, besides the magnetostatic broadening mechanism, another broadening mechanism (the dynamic one) will act. Let us consider two processing dipoles with oppositely directed moments. Each of them will create at the other's location a periodic field of the resonance frequency, under whose influence an exchange of orientation of the moments is possible, since the total energy is conserved in this case. The limitation of the lifetime of each particle in a given Zeeman energy level leads to a broadening of the resonance line which is of the order of $h/\beta^2 r^{-3}$. In other words, "spin-lattice relaxation" mechanisms produce an equilibrium population of the Zeeman states and effectively broadens the resonance line. Spin diffusion[26] corresponds to a spatial propagation of spin magnetization through the simultaneous flipping of nearby spins. It is easy to envisage that such a diffusion allows for broadening of the resonance line.

An inhomogeneously broadened resonance line, on the other hand, is one which consists of a spectral distribution of individual resonant lines merged into one overall line or envelope. The most prosaic source of inhomogeneity of the line broadening is the lack of homogeneity of the applied magnetic field. If such inhomogeneities over the sample exceed the natural linewidth, then the spins in various parts of the sample will find themselves in different field strengths and the resonance will be artificially broadened in an inhomogeneous manner.

Other sources of inhomogeneous broadening include unresolved hyperfine structure, unresolved fine structure, crystal lattice irregularities (e.g. mosaic structure), and the dipolar interactions between unlike spins, i.e. spins with different Larmor frequencies.

The most important homogeneous line broadening mechanisms are the dipolar[27] and exchange interactions[28]. These are treated in detail by Van Vleck[28] in his early paper and in a more concise form in his review article entitled "Line-Breadths and the Theory of Magnetism"[29]. The method that Van Vleck used in his analysis of the shape of the paramagnetic resonance absorption line was "the method of moments", which was first proposed by Waller[30], and which will be considered in some detail later on. Firstly, a few definitions of some of the concepts, necessary to be in acquaintance with, in order to follow Van Vleck's paper, will be given.

AREA AND MOMENTS OF A RESONANCE ABSORPTION CURVE

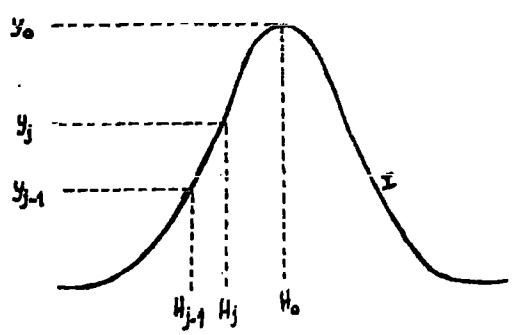

The area A under the resonance absorption curve I, as illustrated, is given by[19]

$$A = \sum_{j=1}^{m} y_j \, (H_j - H_{j-1})$$

where y_j is the amplitude of the resonance absorption line at the magnetic field H_j. In practice it is convenient to select equal

intervals $(H_j - H_{j-1})$ along the field direction so that

$$A = (H_j - H_{j-1}) \sum_{j=1}^{m} y_j$$

where there are m intervals in all. This area is usually proportional to the number of unpaired spins in the sample. The precision of the area determination is increased by increasing m and decreasing the interval $(H_j - H_{j-1})$.

The n-th moment $\langle H^n \rangle$ of a resonance absorption is defined by

$$\langle H^n \rangle = \frac{H_j - H_{j-1}}{A} \sum_{j=1}^{m} (H_j - H_o)^n y_j$$

where the summation limits are the same as before and, in general, these moments are functions of the field H_o. If a resonance absorption line is symmetrical, then the first moment and all other odd moments vanish for the proper choice of H_o.

In terms of integrals, these equations become

$$A = \int_{-\infty}^{\infty} Y \, dH = 2 \int_{o}^{\infty} Y \, dH$$

and

$$\langle H^n \rangle = \begin{cases} 0 & n \text{ odd} \\ (2/A) \int_{o}^{\infty} (H - H_o)^n Y \, dH & n \text{ even} \end{cases}$$

Similar equations for the situation in which derivatives of the absorption line are obtain (which is the most common case in ESR spectrometers) can be found in the reference already quoted. Moreover, bearing in mind the relationship between magnetic field and frequency via the resonance equation ($h\nu = g\beta H$), all these equations can be written in terms of frequency which is precisely the nomenclature used by Van Vleck.

THE GAUSSIAN MODEL

A more appropriate approach to the description of line structure in solids is furnished by the so-called statistical theory, which assumes that the effect of other atoms on a given atom can be approximated by a static field rather than represented by a sudden impact, as suggested by Lorentz in his phase interruption model, which is applicable for treating the shape of collision-broadened lines in gases but which loses its validity when dealing with solids. The shape of the line in the statistical theory is determined by the distribution of magnetic fields over a variety of atoms. If a given atom interacts with a large number of neighbours, so that the total field is compounded from a large number of small fields, the distribution of resultant fields should presumably be approximately Gaussian, for the Gaussian situation is a quite general consequence of the statistics of the aggregates of a large number of objects. This is actually the situation in the case of solids composed of regularly spaced atoms in which the only interactions between the moments of different atoms are dipolar ones which vary slowly with distance, so that a given atom feels the influence of many atoms. It should, however, be mentioned that the statistical theory does not necessarily imply Gaussian distribution, and vice versa.

The Gaussian expression for the line shape normalized to unity is[29]

$$f(\omega) = \left[\frac{1}{2\pi\langle\Delta\omega^2\rangle_{AV}}\right]^{1/2} \exp\left[-(\omega-\omega_o)^2/2\langle\Delta\omega^2\rangle_{AV}\right]$$

There is only a single parameter, viz. the mean square deviation $\langle\Delta\omega^2\rangle_{AV}$ from the mean or central angular frequency ω_o. It is fairly easy to calculate this parameter by the method of moments whilst the "eigenvalue problem" connected with the interaction of a large number of spins is very difficult to analyse exactly.

VAN VLECK'S METHOD OF MOMENTS

The classical interaction energy E between two magnetic moments $\bar{\mu}_1$ and $\bar{\mu}_2$ is [30]:

$$E_d = \frac{1}{r^3}\bar{\mu}_1 \cdot \bar{\mu}_2 - \frac{3}{r^5}(\bar{\mu}_1 \cdot \bar{r})(\mu_2 \cdot \bar{r})$$

where $\bar{r}$ is the radius vector from $\bar{\mu}_1$ to $\bar{\mu}_2$. Using the well known relationship $\bar{\mu} = g\beta\bar{S}$, where as usual g is the Lande factor and $\bar{S}$ stands for spin, the quantum mechanical Hamiltonian for the dipolar interaction due to N spins can be written in a straightforward way as:

$$H_d = g^2\beta^2 \sum_{j,k=1}^{N}\left[\frac{\bar{S}_j \cdot \bar{S}_k}{r_{jk}^3} - \frac{3(\bar{S}_j \cdot \bar{r}_{jk})(\bar{S}_k \cdot \bar{r}_{jk})}{r_{jk}^5}\right]$$

where, of course, terms with j = k are excluded. The "exchange interaction" energy E_{ex} between two magnetic moments with spin S is usually written

$$E_{ex} = -2J\,\bar{S}_1 \cdot \bar{S}_2 \quad .$$

where J is referred as the "exchange integral".

Under the assumptions that (i) the only interactions between the spins of the different atoms are dipolar and exchange couple, (ii) all atoms have the same spins, and (iii) the crystalline Stark energy has no effect on the line breadth, Van Vleck added the equations for H_d and E_{ex} plus the Zeeman contribution to obtain as a Hamiltonian:

$$H = \underbrace{g\beta\bar{H} \cdot \sum_j \bar{S}_j}_{\text{Zeeman Energy}} \underbrace{- 2\sum_{k>j} J_{jk}\,\bar{S}_j \cdot \bar{S}_k}_{\text{Exchange Energy}} + \underbrace{g^2\beta^2 \sum_{k>j}\left[\frac{\bar{S}_j \cdot \bar{S}_k}{r_{jk}^3} - \frac{3(r_{jk} \cdot S_j)(\bar{r}_{jk} \cdot \bar{S}_k)}{r_{jk}^5}\right]}_{\text{Dipolar Energy}}$$

One should note that the first term in the dipolar energy has the same form as the exchange interaction, however, the exchange part J_{jk} falls off with the distance much more rapidly than r_{jk}^{-3}, and is effective

only for nearest or next nearest neighbours. In contrast to J_{jk}, the second term in the dipolar energy is strongly dependent on the orientation of the dc magnetic field relative to the crystallographic axis.

As mentioned before, the result of the simultaneous interaction of many, many spins, produces a Gaussian shaped resonant line and the difficulty of its analysis was overcome by Van Vleck who expanded the Hamiltonian in terms of the "ladder" operators $S^+ = S_x + iS_y$ and $S^- = S_x - iS_y$ and found that this Hamiltonian could be "truncated", provided the Zeeman energy is large compared to the dipolar and exchange interactions, for it was shown that the effect of the omitted part is to generate weak transitions (or satellites) whose frequencies are near 0, $2g\beta H/h$, $3g\beta H/h$ and which are not possible to observe at high magnetic fields. Using this truncated Hamiltonian he found that, for like atoms, the second moment, $\langle \Delta\omega^2 \rangle$, can be written

$$\langle \Delta\omega^2 \rangle = \frac{3}{4} S(S+1) (g^2\beta^2/\hbar)^2 \cdot n \cdot \sum_k \left[r_{jk}^{-6} \, (3\cos^2\theta_{jk} - 1)^2 \right]$$

where ω is measured in radians per second, n is the concentration of interacting atoms, g is the Lande factor, β is the Bohr magneton, r_{jk} is the radius vector from the reference atom j to all the neighbouring atoms labelled over k, and θ_{jk} is the angle between the radius vector and a crystallographic reference axis.

For unlike atoms the equation becomes

$$\langle \Delta\omega^2 \rangle = \frac{1}{3} S(S+1) (gg'\beta^2/\hbar)^2 \cdot n \cdot \sum_k \left[r_{jk}^{-6} \, (3\cos^2\theta_{jk} - 1)^2 \right]$$

where g refers to the reference atom and g' to the second species; n is the concentration of the latter.

The term between brackets [ ] is a pure geometrical factor, i.e. dependent on the crystal structure, and can be evaluated using spherical harmonics, Y_{lm}, following the procedure which has been employed by G. Brown et al[1].

For a crystal of cubic symmetry the equations for the second moment are:

(a) for like atoms

$$\langle\Delta\omega^2\rangle = \frac{3}{4} S(S+1)\left(g^2\beta^2/\hbar\right)^2 \cdot n \left[\frac{4}{5}\sum_k\left(r_{jK}^{-6}\right)\right.$$

$$+ \frac{32\pi}{35} Y^*_{4,0}\left(\theta_H,\phi_H\right) \sum_k r_{jK}^{-6} Y_{4,0}\left(\theta_K,\phi_K\right)$$

$$+ \frac{32\pi}{35} Y^*_{4,4}\left(\theta_H,\phi_H\right) \sum_k r_{jK}^{-6} Y_{4,4}\left(\theta_K,\phi_K\right)$$

$$\left. + \frac{32\pi}{35} Y^*_{4,-4}\left(\theta_H,\phi_H\right) \sum_k r_{jK}^{-6} Y_{4,-4}\left(\theta_K,\phi_K\right)\right]$$

(b) for unlike atoms

$$\langle\Delta\omega^2\rangle = \frac{1}{3} S(S+1)\left(gg'\beta^2/\hbar\right)^2 \cdot n \left[\frac{4}{5}\sum_k\left(r_{jK}^{-6}\right)\right.$$

$$+ \frac{32\pi}{35} Y^*_{4,0}\left(\theta_H,\phi_H\right) \sum_k r_{jK}^{-6} Y_{4,0}\left(\theta_K,\phi_K\right)$$

$$+ \frac{32\pi}{35} Y^*_{4,4}\left(\theta_H,\phi_H\right) \sum_k r_{jK}^{-6} Y_{4,4}\left(\theta_K,\phi_K\right)$$

$$\left. + \frac{32\pi}{35} Y^*_{4,-4}\left(\theta_H,\phi_H\right) \sum_k r_{jK}^{-6} Y_{4,-4}\left(\theta_K,\phi_K\right)\right]$$

θ_K and ϕ_K refer the radius vector to the crystal axes while θ_H and ϕ_H refer the static magnetic field to the same axes.

THE MAGNESIUM OXIDE UNIT CELL

The unit cell of Magnesium Oxide, as previously mentioned in Chapter II, is face centred cubic and contains four molecules (see Figure 2.1). The iron is expected to substitute at the magnesium sites and so a complete tabulation of these sites is needed. It is found sufficient to consider eight unit cells with the iron reference

ion as a common corner. The r, θ, ϕ values of all the magnesium sites are given in the Appendix (see Table 1).

Because of the symmetrical properties of the crystal structure these equations reduce at $\phi_H = 0^\circ$ (which is the case considered here) to:

(a) for like atoms

$$\langle\Delta\omega^2\rangle = \frac{3}{4} S(S+1)\left(g^2\beta^2/\hbar\right)^2 \cdot n \cdot \left[\frac{4}{5}\sum_K\left(r_{jK}^{-6}\right) + \right.$$
$$+ \frac{32\pi}{35} Y^*_{4,0}(\theta_H,\phi_H)\sum_K r_{jK}^{-6} Y_{4,0}(\theta_K,\phi_K)$$
$$\left. + \frac{64\pi}{35} Y^*_{4,4}(\theta_H,\phi_H)\sum_K r_{jK}^{-6} Y_{4,4}(\theta_K,\phi_K)\right]$$

(b) for unlike atoms

$$\langle\Delta\omega^2\rangle = \frac{1}{3} S(S+1)\left(gg'\beta^2/\hbar\right)^2 \left[\frac{4}{5}\sum_k\left(r_{jK}^{-6}\right)\right.$$
$$+ \frac{32\pi}{35} Y^*_{4,0}(\theta_H,\phi_H)\sum_K r_{jK}^{-6} Y_{4,0}(\theta_K,\phi_K)$$
$$\left. + \frac{64\pi}{35} Y^*_{4,4}(\theta_H,\phi_H)\sum_K r_{jK}^{-6} Y_{4,4}(\theta_K,\phi_K)\right]$$

The total dipolar broadening is given by the square root of the sum of the second moments of the individual dipolar interactions. This mean square width must be converted into the peak to peak derivative linewidths, ΔH_{ms}, for comparison with experimental results. This is done using the equation

$$\Delta H_{ms} = \frac{\sqrt{\langle\Delta\omega^2\rangle}}{\pi} \cdot {}^{\partial H}/_{\partial\nu} \qquad \text{Tesla}$$

where the parameter ${}^{\partial H}/_{\partial\nu}$ is obtained from the experimental isofrequency plots obtained for each crystal. One of these is shown in Figure 4.2 for a concentration 0.3106% (i.e. 4300 p.p.m. of Fe), and the transition indicated.

For the iron-iron interactions one needs the equation for dipolar broadening between like atoms. For Fe^{3+}, S = 5/2 and g = 2.0037, the atomic part of the equation can be evaluated as

$$\frac{3}{4} S(S+1) \left(g^2\beta^2/\hbar\right)^2 \cdot n = 7.0621 \times 10^{-25} \cdot n \text{ rad.sec}^{-1} \text{ cm}^6$$

Using Table 2 the geometrical part of the equation can be partially evaluated, leading to the final equation:

$$\langle\Delta\omega^2\rangle = 7.062 \times 10^{20} \, n \left[15.9184 - 5.175 \, Y^*_{4,0}(\theta_H,\phi_H) - 6.218 \, Y^*_{4,4}(\theta_H,\phi_H)\right]$$

For $\phi = 0^\circ$ the equation is totally real and by substituting values of n and θ corresponding to the experimental ones, curves of dipolar broadening as a function of polar angle, θ, can be derived. Using the equation of transformation; ΔH_{ms} can be calculated and compared with experimental values. It should be noticed that the dipolar interaction between Fe and Mg, and Fe and Oxygen give a negligible contribution to the broadening of the lines.

The predicted concentration dependence of the linewidth is shown in Figure 4.7 which also shows the experimental data obtained with the "as received" samples.

IV.2 EXPERIMENTAL RESULTS

The experimental results to be presented in this section are to be classified as those obtained with the samples "as received", and after heat treatment either in an oxidizing or reducing atmosphere. By "as received" is meant the crystals as they were supplied by the manufacturers whilst by "heat treated" samples it should be understood that the crystals were re-examined after a baking process.

A typical spectrum, obtained with the as received samples at room temperature at a frequency of 9.100 GHz and polar angle $\theta = 0^\circ$

(i.e. external magnetic field H parallel to the fourfold axis of the crystal) is shown in Figure 4.1. The spectrum shows a total of five lines, which is the correct number expected for S = 5/2 if it is Fe^{3+}, and there is a general agreement with that reported by Low[7] in the 1.15 centimeter region. The $\frac{1}{2} \leftrightarrow -\frac{1}{2}$ transition appears as a prominent line of relative intensity 11.5 at approximately g = 2.016 flanked on either side by two lines at separations 443 and 545 Gauss respectively and with relative intensities 0.5 and 2.2.

The spectrum shown in Figure 4.1 corresponds to that obtained with the sample containing, nominally 0.03% of iron (sample ref. No.2) and it is similar for most of the other samples; with two however (ref. Nos. 1 and 3) six extra lines were observed and it is not known whether these were due to impurities or iron ions located in sites of lower symmetry. Table II shows a summary of the field positions and relative intensities of the five lines as found experimentally with the sample ref. No.2

TABLE II

Experimental spectrum of the $MgO:Fe^{3+}$ at 9.100 GHz and H // <100>-axis

Transition	$-\frac{1}{2} \leftrightarrow -3/2$	$5/2 \leftrightarrow 3/2$	$\frac{1}{2} \leftrightarrow -\frac{1}{2}$	$-3/2 \leftrightarrow -5/2$	$3/2 \leftrightarrow \frac{1}{2}$
H_{res} (Gauss)	2710	2810	3225	3668	3770
Rel. Inten.	2.2	0.5	11.5	0.5	2.2

By comparison of Tables I and II it can be seen that the predicted spectrum is in fairly good agreement with the experimental one.

The main transition, i.e. $\frac{1}{2} \leftrightarrow -\frac{1}{2}$, was used for detailed line-width studies. The reasons for this choice were twofold: (a) its intensity was greater, and (b) it was nearly isotropic. The second point was made clear from isofrequency plots.

For the $-\frac{1}{2} \leftrightarrow -3/2$ and $3/2 \leftrightarrow \frac{1}{2}$ transitions, as Figure 4.2 shows, there is a large variation of resonance magnetic field as the polar angle θ is varied and at some angles they overlap with the main transition. The $\frac{1}{2} \leftrightarrow -\frac{1}{2}$ isofrequency plot, however, as illustrated in Figure 4.3, shows a very much smaller variation. It does not, however, appear to be exactly isotropic as has been previously suggested by Low[7] and, in fact, shows certain periodic maxima and minima. The pattern of variation is very similar to that reported by Toussaint and Declerck[31] for the case in which the magnetic field is directed along the <111> axis of the crystal. Moreover, these researchers have shown that the resonance magnetic field changes by up to 40 Gauss as the polar angle is varied from $\theta = 0^{\circ}$ to $\theta = 90^{\circ}$ which, as can be seen in Figure 4.3, is very much the same range of values of magnetic field reported here for the $\frac{1}{2} \leftrightarrow -\frac{1}{2}$ transition and for the magnetic field along the fourfold axis of the crystal.

The linewidth of the $\frac{1}{2} \leftrightarrow -\frac{1}{2}$ transition for each one of the samples was measured directly from the derivative plot (e.g. Figure 4.4) which was calibrated in terms of magnetic field as was explained in the preceding chapter. The variation of linewidth with polar angle is shown in Figure 4.5(a) for several samples; all in fact showed a definite minimum near $\theta = 0^{\circ}$, and an increase in linewidth of nearly two times on going to $\theta = 20^{\circ}$. Actually, on going further up varying the polar angle the linewidth decreases and increases periodically but these experimental points are a bit doubtful in the region in which this transition overlaps with the $-\frac{1}{2} \leftrightarrow 3/2$ and $3/2 \leftrightarrow \frac{1}{2}$ transitions, since its amplitude decreases radically and the measurement of the linewidth becomes impossible. Nonetheless, as can be appreciated from Figure 4.5(b), there appear to be points of maxima and minima for the linewidth at values of θ quite similar to those found in the isofrequency plot of the main transition.

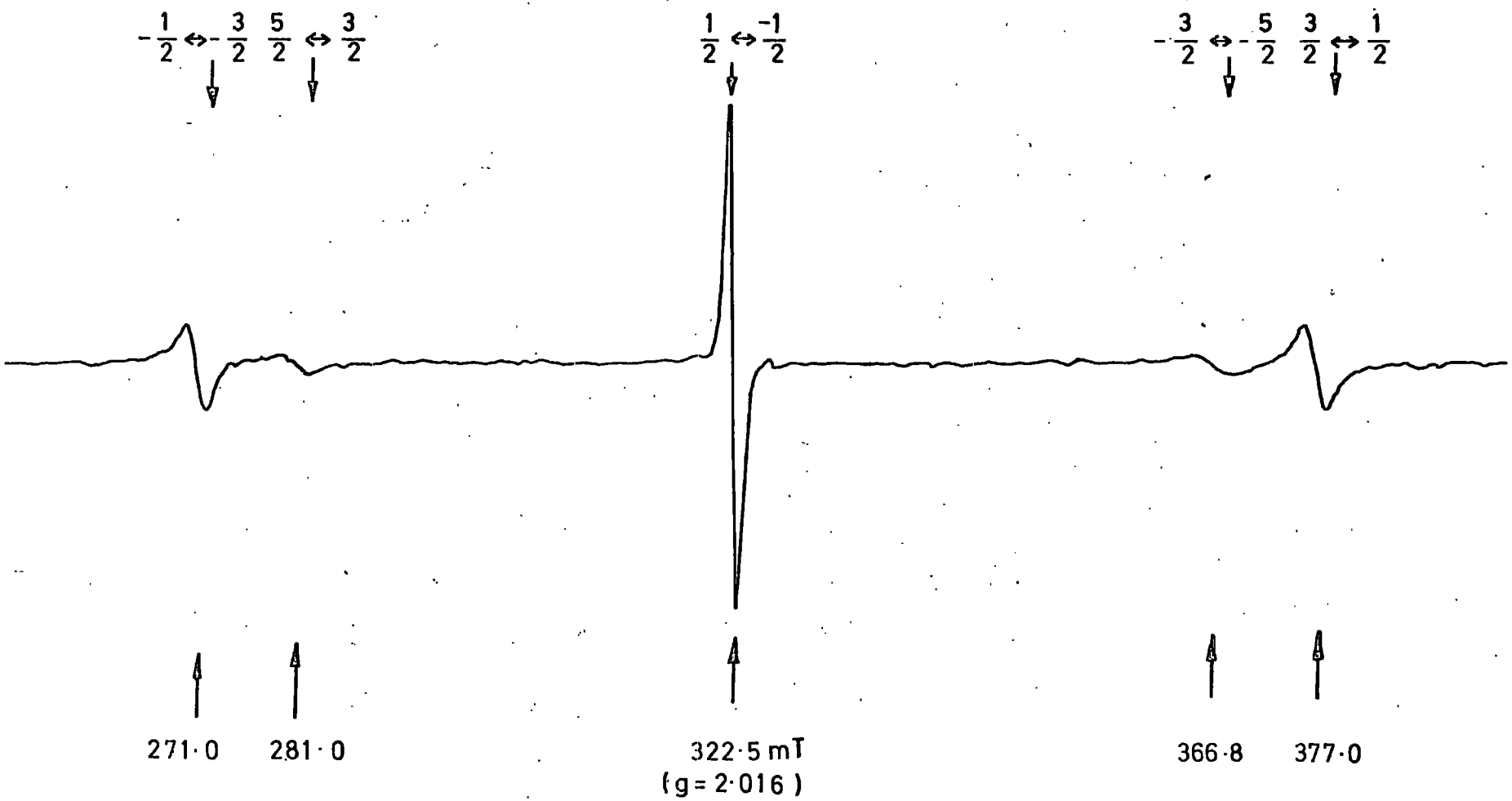

FIG. 4·1. E.S.R. spectrum of Fe^{3+}/MgO; room temperature, $\Theta_H = 0°$, 9·10 GHz, 310 ppm Fe.

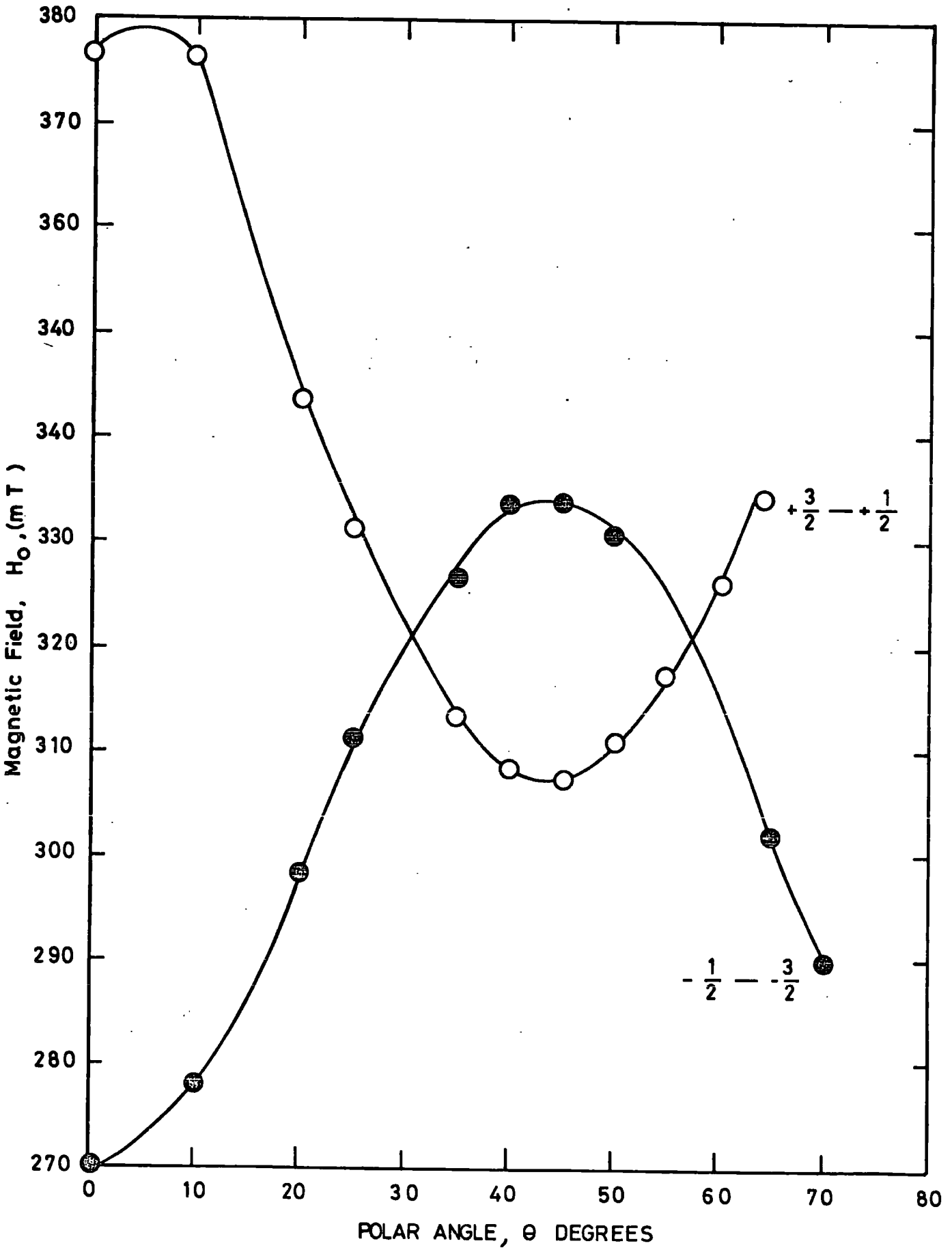

FIG 4·2. Isofrequency plot for Fe^{3+}/MgO ; 9·090 GHz, 293 K, 4300 ppm Fe.

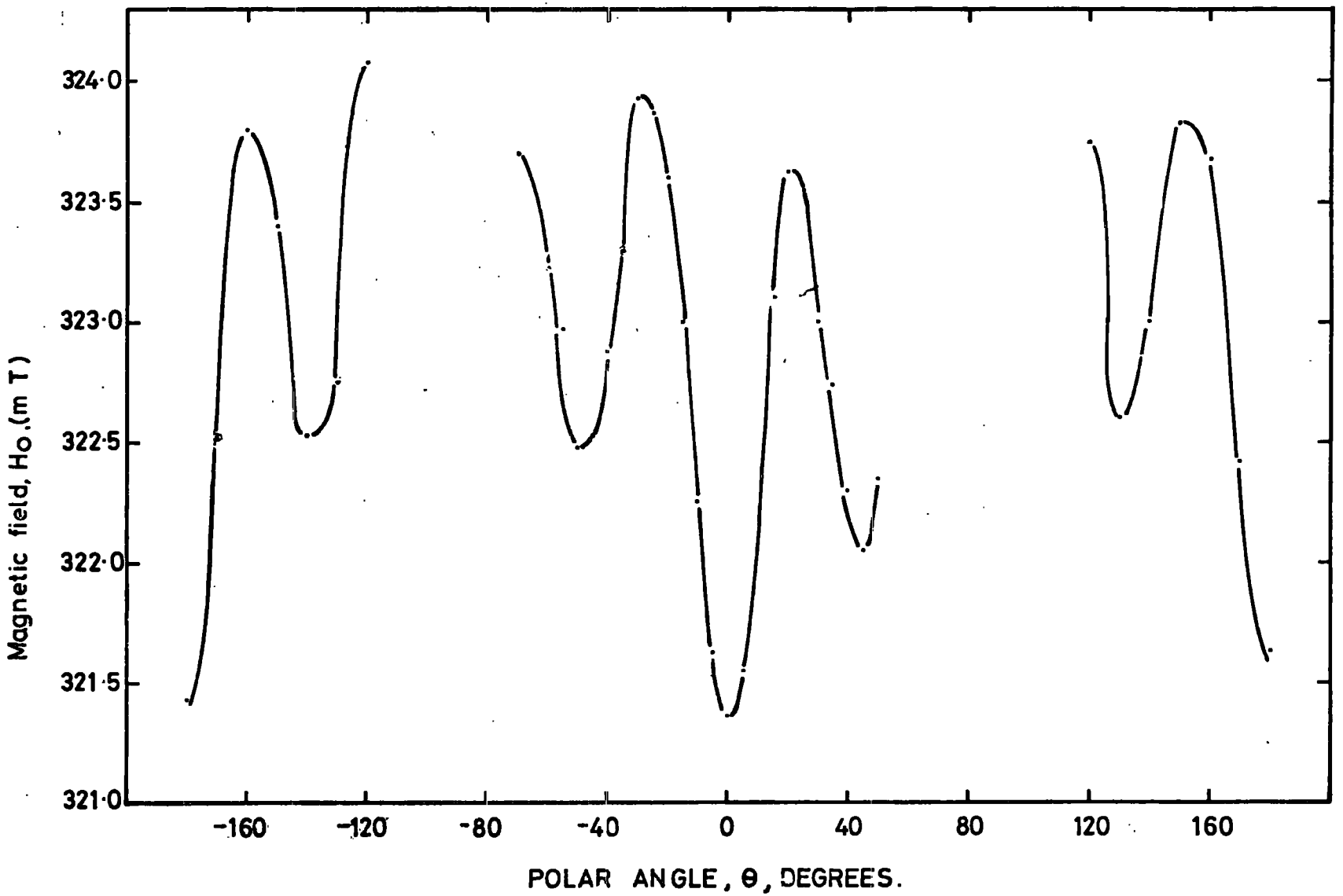

FIG 4·3 Isofrequency plot of the $\frac{1}{2} \leftrightarrow \frac{1}{2}$ transition for MgO: Fe^{3+} (4300 ppm Fe), room temperature, 9·090 GHz.

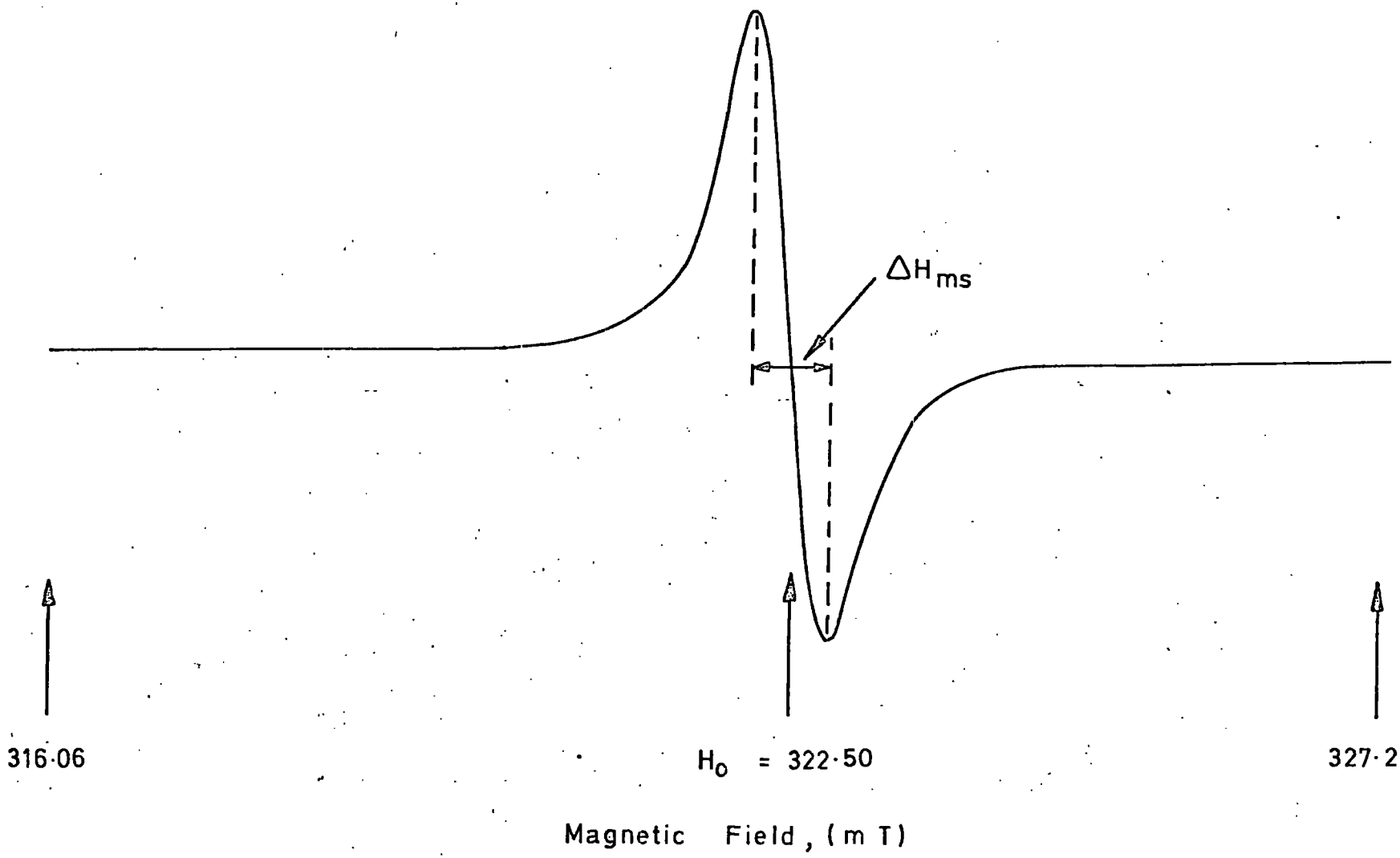

FIG. 4·4 Lineshape of $\frac{1}{2} \leftrightarrow -\frac{1}{2}$ transition in Iron doped Magnesium Oxide; room temperature, 9·100 GHz, $\Theta = 0°$, 310 ppm Fe.

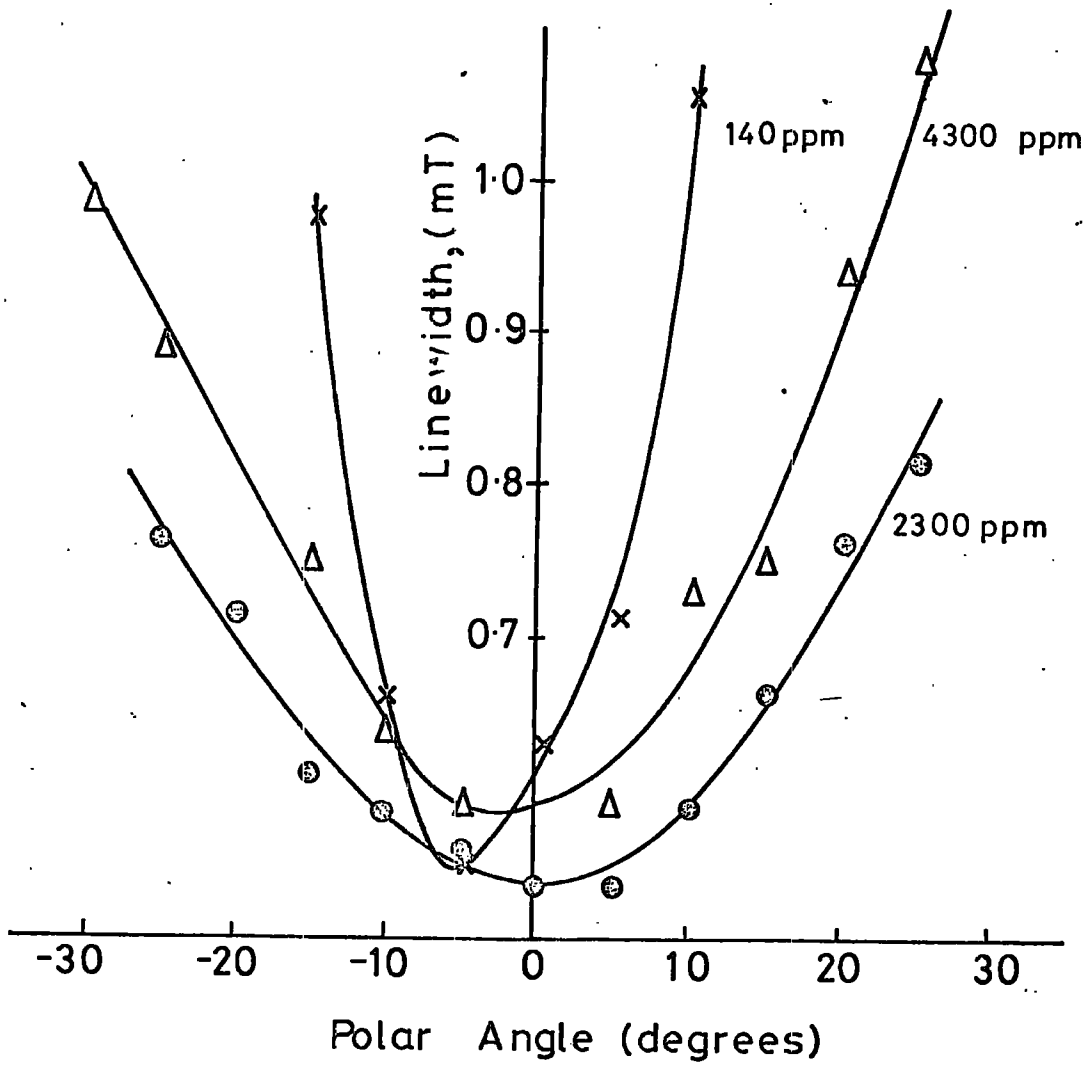

FIG 4·5.(a). Linewidth variation with polar angle, ($\theta < 30°$); 77 K, 9·0 GHz.

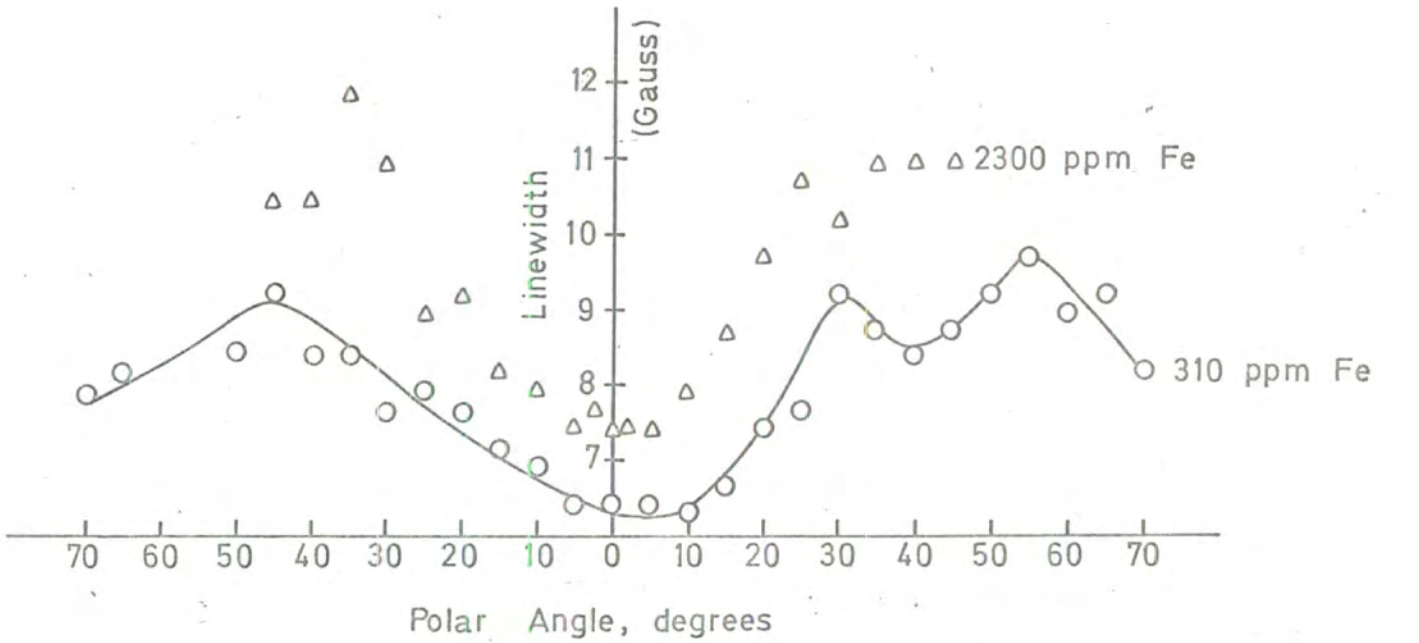

FIG. 4·5 (b) Linewidth versus polar angle, $\frac{1}{2} \leftrightarrow \frac{1}{-2}$ transition, Fe^{3+}/MgO, room temperature, 9·1 GHz.

The experimental linewidth, measured at room temperature, was found to be almost the same for all the samples and it is approximately of 8 Gauss at $\theta = 0^{o}$. Measurements were also made at liquid nitrogen temperature to check whether there was any appreciable contribution to the linewidth due to broadening caused by spin-lattice relaxation (which will be treated in the next chapter). The full spectra were identical with that shown in Figure 4.1 and the linewidth was similar to that measured at room temperature; thus, such an effect was considered negligible. A plot of linewidth versus concentration is shown in Figure 4.6 which also includes 77 K results obtained with the same samples and it can be seen that the linewidth seems to be independent of concentration.

Using Van Vleck's theory of dipolar broadening, outlined in the previous section, a calculation of the expected linewidth was performed and, as can be appreciated from Figure 4.7, the discrepancy between the theoretical and experimental values was significant. Three main suppositions were proposed to account for this difference in linewidth: either (a) from the total nominal concentration of the dopant only-a small part was in the trivalent state and, consequently, the figures adopted for the Fe^{3+} concentration led to erroneous calculations or (b) the existence of small amounts of the fast relaxing[32,33] Fe^{2+}, interacting somehow with the ferric ion, may cause the shrinkage of the linewidths or (c) both situations taking place at the same time. Optical measurements carried out by W. Hutton revealed the presence of detectable amounts of Fe^{2+} in two of the samples (ref. Nos.4 and 5) whereas the low concentration samples did not show any Fe^{2+} signal at all.

Bearing in mind these assumptions, it was decided to heat treat the samples in air[34] at a temperature above $1200^{o}C$ in order to increase

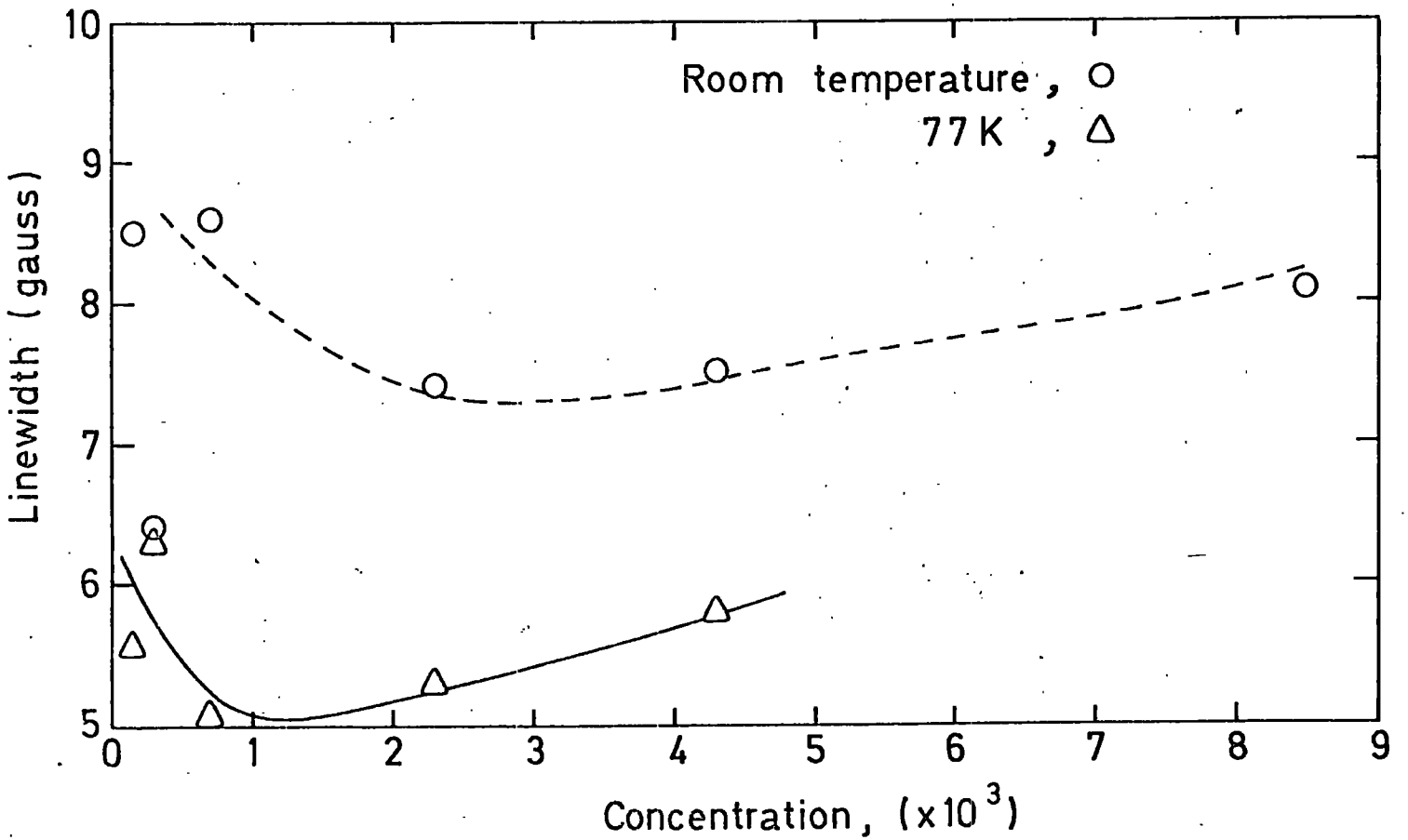

FIG. 4·6. Experimental variation of linewidth with iron concentration; Fe/MgO, $\Theta = 0°$, 9·1 GHz, $\frac{1}{2} \leftrightarrow -\frac{1}{2}$ transition.

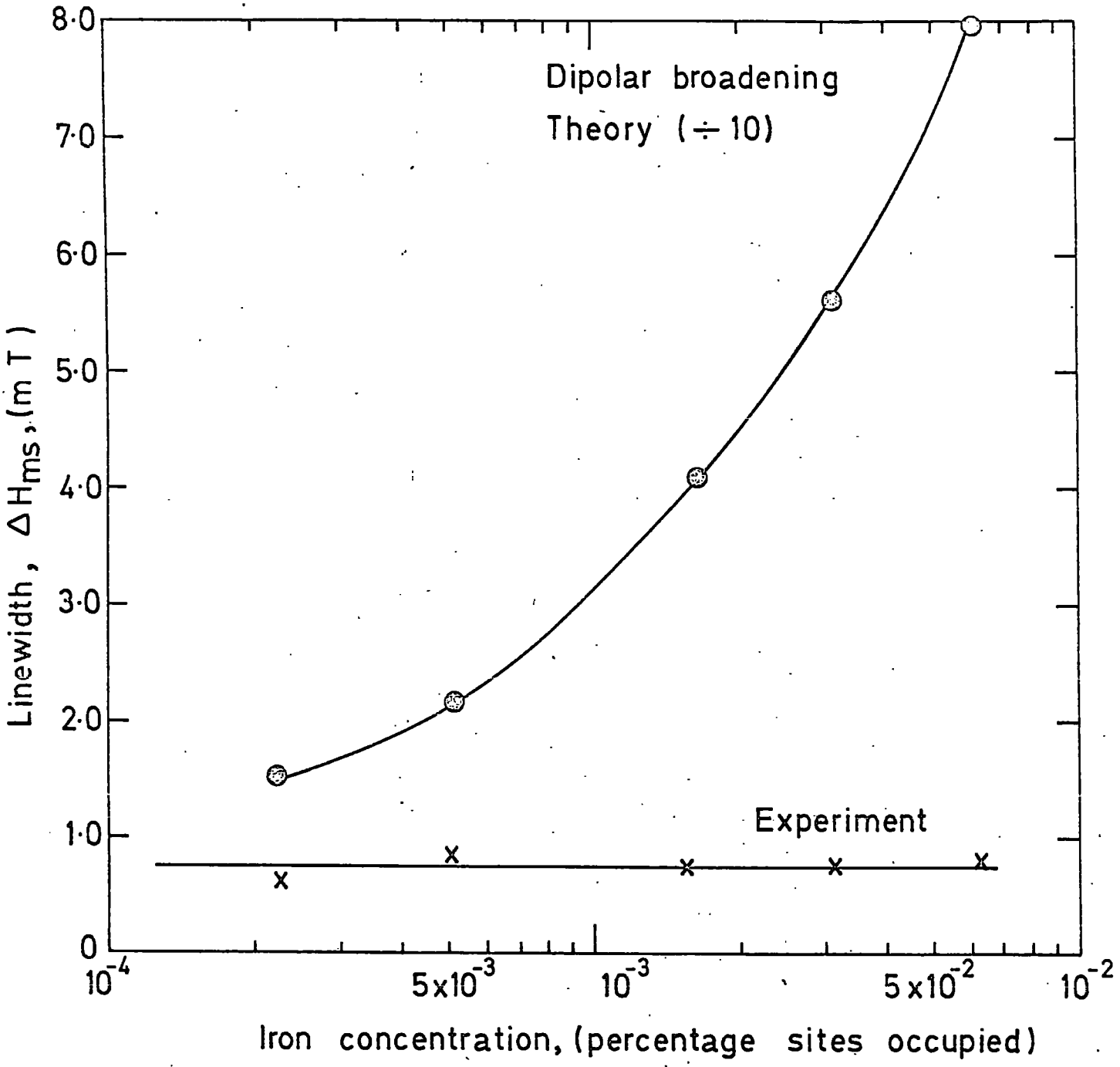

FIG. 4·7. Variation of linewidth with concentration in iron doped MgO; $\frac{1}{2} \leftrightarrow -\frac{1}{2}$ transition, $\Theta_H = 0°$

the ratio of Fe^{3+} to Fe^{2+} and observe whether there was any change in linewidth. Sample ref. Nos.1, 2, 3, 4 and 5 were baked for periods up to 24 hours and then were allowed to cool down at a slow rate. As a result of this heat treatment the green-coloured crystals turned orange (i.e. samples ref. Nos. 4 and 5), the samples containing 140 and 710 p.p.m. of iron turned yellow whilst the 310 p.p.m. sample remained colourless as before the baking process.

As far as the linewidth measurements are concerned, in all the heat treated samples the main transition of the ferric ion showed a slight tendency to increase in linewidth, the major increase measured being of nearly two times for the sample ref. No.5. Further optical spectroscopic measurements were performed with the heat treated samples and it was found that the absorption peaks identified as corresponding to the ferric ion had increased in amplitude, the most intense corresponding to those samples which had changed colour. However, the samples ref. Nos.4 and 5 still showed a very intense peak corresponding to the divalent iron ion.

The next obvious step was to proceed to analyse the samples in a situation in which the Fe^{2+} ion dominates in proportion to the ferric ion and so the crystals were once again baked but this time in a Hydrogen atmosphere for periods up to 30 hours. As a consequence, the samples ref. Nos.4 and 5 "returned" to their original dark-green colour, but the low concentration ones became completely transparent. Linewidth measurements in the former gave as a result a value equal to that obtained when measured in the as received state, but the latter did not show Fe^{3+} spectrum at room temperature at all. As before, the optical spectrum of the Hydrogen treated samples was obtained: the samples ref. Nos.4 and 5 still showed the Fe^{3+} absorption peaks in addition to the Fe^{2+} peak, but

the low concentration samples showed neither Fe^{3+} peaks nor Fe^{2+} peaks. However, at Q-band and liquid helium temperature these low concentration samples showed a rather weak Fe^{3+} spectrum and an intense broad line at about 7.5 Kilogauss which was identified as corresponding to a Fe^{2+} transition by comparison with the spectrum reported by Low and Weger[35].

IV.3 DISCUSSION AND CONCLUSIONS

Two salient features emerge from an initial comparison between the experimental result for the as grown crystals and those predicted on the basis of Van Vleck's dipolar broadening theory. Firstly, the expected linewidths are about a hundred times larger than the measured linewidths; secondly, the linewidth appears to be almost concentration independent, in marked contrast to the $(\text{concentration})^{\frac{1}{2}}$ variation expected.

The discrepancy in the magnitude of the linewidths is far greater than those encountered in other materials in which similar comparisons have been made. In ruby, for example, Grant and Strandberg[36] found that the predicted dipolar widths were some five times larger than the observed widths; and in a recent publication on double doped alumina Thorp et al[37] found that the predicted widths were seven times larger than those observed. In these examples, however, there was a reasonably good fit between the forms of the predicted and observed angular variation of the linewidth and also between the predicted and observed linewidth concentration dependence. With the present data only the form of the angular variation of linewidth corresponds to the predictions of the dipolar model.

At this stage of the research, to account for the above mentioned discrepancy, it was suggested that either (a) incorrect Fe^{3+} concentration

figures, or (b) the presence of Fe^{2+} interacting with the Fe^{3+} ions, or (c) both considerations, may explain the "shrinkage" of the linewidth. However, in the light of the additional data obtained with the heat treated samples, a more consistent suggestion arose in order to explain the remarkable difference between the predicted and the observed linewidth: existence of a strong narrowing mechanism such as, for example, exchange[38] or motional[39] narrowing. These possibilities are discussed below.

As regards the Fe^{3+} concentrations the figures used, obtained by spectrographic analysis, referred to the total iron content. This method of analysis did not differenciate between various valency states and it was possible that although the crystals certainly contained Fe^{3+}, as shown by the E.S.R. spectra, they might also contain other states such as Fe^{2+}. However, the dipolar calculations can be used to obtain by extrapolation the concentration of Fe^{3+} which would have been needed to account on the dipolar model for the observed 8 Gauss linewidth. This extrapolation gives a required concentration of only 0.53 p.p.m. of Fe^{3+}. Even allowing for a substantial percentage of the total iron content being present as species other than Fe^{3+}, this extremely low value makes it very unlikely that the linewidth discrepancy could be explained purely on concentration grounds; furthermore, no explanation of the concentration independent linewidths would be afforded without an unlikely assumption that the Fe^{3+} concentration remained low and constant although the total iron content increased from 140 p.p.m. to 12900 p.p.m. Moreover, after heat treatment in air the intensity of the Fe^{3+} E.S.R. spectrum was, in most specimens, somewhat more pronounced and the linewidths tended to increase but only by factor of less than two times; even in the situation where maximum conversion of Fe^{2+} into

Fe^{3+} had been attempted (after prolonged heating in air) the linewidths were still much less than the predicted values.

The optical absorption in several of the present specimens has been studied over the range 200 nm to 1000 nm. In the as received state all the specimens showed peaks at 395 nm and 462 nm which agree with the values quoted by Wertz et al[34] for the absorption peaks of Fe^{3+} in iron doped-magnesia, and which increased progressively with total iron concentration. Only two samples, those containing 2300 p.p.m. and 4300 p.p.m. Fe respectively, gave in addition a broad absorption centred near 1000 nm which agrees with the value reported by Jones[40], and confirmed later by Cotton et al[41] and King et al[42], for an absorption peak of Fe^{2+} in octahedral co-ordination. Hence, it is concluded from this optical data that while all the specimens contained Fe^{3+}, only in the two specimens noted above existed a detectable amount of Fe^{2+}. Nevertheless, since small decreases in linewidth were seen after the heat treatment of the samples in a hydrogen atmosphere, it is concluded that the Fe^{2+} does not play the most important role in the behaviour of the linewidth of the $\frac{1}{2} \leftrightarrow -\frac{1}{2}$ transition of the ferric ion.

An explanation in terms of exchange narrowing seems more likely since this would involve an interaction between ions of like species which here would be Fe^{3+} - Fe^{3+}. From the equation for the second moment it is apparent that the isotropic exchange forces do not influence at all the magnitude of the second moment. In order to determine the influence of exchange forces on the line shape, it is therefore necessary to consider higher moments. Calculations have shown that in the case of pure dipolar interactions the ratios of the moments are close to the values obtained for Gaussian functions, namely

$$M_6^{\frac{1}{6}} : M_4^{\frac{1}{4}} : M_2^{\frac{1}{2}} = 1.57 : 1.32 : 1$$

Al'tshuler and Kozyrev[10] had mentioned that if exchange interactions are stronger than the dipole interactions, the

$$M_4^{\frac{1}{4}} : M_2^{\frac{1}{2}} >> 1$$

where M_2 and M_4 are respectively the second and fourth moments of the line. An analysis of this type has been attempted in the following way. Each absorption line shape was first found by numerical integration of the experimental derivative plots; however the presence of a weak subsidiary line, presumably made that on the high field side the absorption line adopted a form similar to that illustrated by Zavoisky[43] for the exchange narrowed line of $CrCl_3$ polycrystalline samples; thus, it was impossible to obtain data in the high field tail and consequently estimates of M_2 and M_4 were only made for the left hand side of the line where the tail could be followed continuously into the background. The ratio $M_4^{\frac{1}{4}}/M_2^{\frac{1}{2}}$ was then derived. The results, for the Fe^{3+} $\frac{1}{2} \leftrightarrow -\frac{1}{2}$ transition at X band and $\theta = 0^{\circ}$, are summarized in Table III.

TABLE III

Values of the ratio $M_4^{\frac{1}{4}}/M_2^{\frac{1}{2}}$ for the $\frac{1}{2} \leftrightarrow -\frac{1}{2}$ transition of $MgO:Fe^{3+}$

Iron concentration (p.p.m.)	Ratio $M_4^{\frac{1}{4}}/M_2^{\frac{1}{2}}$
140	1.34
310	1.36
710	1.33
2300	1.48
4300	1.42
8500	1.35

The values of the ratio found are not dissimilar to the figures quoted by Van Vleck[29] for other examples of exchange narrowed E.S.R.

lines, e.g. in undiluted paramagnetic salts of Mn^{2+}. For the purpose of illustration Van Vleck's table is reproduced here.

Substance	Exp. Linewidth (Gauss)	Theor. Linewidth (Gauss)	$M_4^{\frac{1}{4}}/M_2^{\frac{1}{2}}$
$MnCl_2.4H_2O$	1410	1530	1.23
$MnCl_2$	750	2950	1.40
$MnSO_4.4H_2O$	1150	1560	1.28
$MnSO_4.1H_2O$	320	2870	1.46
$MnSO_4$	665	3520	1.35
$MnCO_3$(cryst.)	460	4460	1.43
$Mn_3(PO_4)_2.3H_2O$	465	1246	1.38
$Mn_2P_2O_7.3H_2O$	1070	1250	1.32
$Mn(NO_3)_2.6H_2O$	1210	1033	1.31
MnF_2	470	7020	1.39
MnS	780	7520	1.40

(After J.H. Van Vleck, reference 29, pp.1002)

From Van Vleck's figures it could be observed that wherever there is a substantial difference between the calculated and measured linewidths, the value of the moments ratio is quite similar to those produced in Table III. This suggests that exchange narrowing is important, even at the lowest iron concentration. The exchange model might also give an explanation for the concentration independent linewidths. Increasing the iron concentration will increase the probability of the number of magnesium sites being occupied by Fe^{3+} and, consequently, reduce the Fe^{3+} - Fe^{3+} distance and simply correspond to a larger number of centres each producing a stronger narrower effect; thus the concentration independence of the linewidth is to be regarded as the maintenance

of the domination of exchange narrowing over dipolar broadening at all levels of iron concentration.

On the above basis one might expect that the linewidth behaviour of the Fe^{3+} should be substantially independent of any Fe^{2+} present; however, we cannot rule out the possibility of some contribution to narrowing arising from motional effects, which have been invoked by Stoneham et al[44] to explain the temperature dependence of the linewidth or iron group ions in MgO in the temperature range near 2 K. This mechanism however would involve an Fe^{3+} - Fe^{2+} interaction and, in view of the small amounts of Fe^{2+} detected in the specimens used in these experiments, seems unlikely to be a dominant factor.

Thus one ought to conclude from the linewidth experiments that the iron enters the magnesium oxide lattice substitutionally (occupying magnesium sites), that the predominant valency state is Fe^{3+} and that even at low iron concentrations there is strong exchange narrowing of the resonance lines.

CHAPTER V

SPIN-LATTICE RELAXATION MEASUREMENTS

The behaviour of a paramagnetic substance in a magnetic field will depend essentially on the interaction of the paramagnetic particles with one another and with the neighbouring diamagnetic particles. These interactions will favour the establishment of a thermodynamic equilibrium, if that equilibrium is disturbed for any reason.

Let a certain pair of energy levels of a spin system be E_1 and E_2 $(E_1<E_2)$, whose populations are set equal to N_1 and N_2. Hence, if the equilibrium state has been attained in a static field H_o and the distribution laws of classical mechanics are applicable, the populations of the individual energy levels are determined by the Boltzmann factor

$$N_2 = N_1 \exp\left[-(E_1 - E_2)/kT\right] \qquad (5.1)$$

where k is the Boltzmann constant and T is the absolute temperature of the system. The populations of the lower energy levels are greater than those of the upper levels; therefore, when a periodic magnetic field with the resonance frequency is switched on, the number of absorption events produced by the field will exceed the number of induced radiation events, and as a result the substance will absorb energy from the periodic field. If this resonance absorption is to continue, there must be some other mechanism which allows electrons in the upper energy state to lose energy and drop back to the lower state. This mechanism must allow energy transfer by interaction with some system other than the incident radiation. If this were not so, the larger number of electrons absorbing energy in the ground state would rapidly tend to equalize N_1 and N_2 and so no further absorption would occur.

Thus, two opposing processes take place in paramagnetic resonance: the periodic magnetic field tends to equalize the populations of the

various magnetic levels, and the internal interactions tend to restore the Boltzmann distribution by conversion of the energy absorbed into heat. This mechanism of restoration is called "relaxation process" and is measured in terms of the relaxation time, which is the time in which an initial excess of energy given to the spins will fall to 1/e or 0.368 of its value.

In order to describe the mechanism whereby a spin system achieves thermal equilibrium within itself and with its surroundings, three processes must be considered: spin-spin relaxation, cross relaxation and spin-lattice relaxation. By spin-spin relaxation is understood the process of achievement of thermal equilibrium within the spin system itself, cross relaxation deals with the attainment of equilibrium between spins of different species and spin-lattice relaxation describes the way in which the spin system transfers energy to the lattice, the latter being the concern of this chapter.

The group led by Gorter and Casimir [45] made the first real attempt to investigate paramagnetic relaxation. They investigated the behaviour of the paramagnetic susceptibility of the sample, when subjected to radio-frequency fields, and determined the maximum rate at which the magnetic moment of the specimen could follow the changing applied field. The situation was analysed by Casimir and du Pre [46] whose hypothesis suggested that the magnetization of a paramagnetic substance could be considered a two-stage process:

(i) Equilibrium is established inside the "spin system", i.e. the system of the magnetic moments of all paramagnetic particles.

(ii) An exchange of energy takes place between the spin system and the "lattice" which comprises all the remaining degrees of freedom of the paramagnetic substance.

According to this thermodynamic approach a system whose temperature is not the same as that of its surroundings cannot certainly be in thermal equilibrium with these surroundings and, provided there is a thermal contact between the two, their temperatures will approach a common value at a rate determined by the heat capacities of the system and the surroundings together with the rate at which energy can be transferred from one to the other. If the surroundings have a heat capacity that is immensely greater than the heat capacity of the system, the temperature of the latter will approach the temperature of the surroundings at a rate determined only by the heat capacity of the system and the rate of heat transfer.

In other words, the lattice acts like a thermostat in which the spin system is immersed since its temperature may be regarded as constant because its heat capacity is much greater than that of the spin system. A certain temperature which is, in general, different from the lattice temperature may also be attributed to the spin system.

The process of establishing an equilibrium between the spin system and the lattice may be considered as an exchange of energy between the systems, leading to temperature equalization. The rate of this process may be characterized by the spin-lattice relaxation time, which will be denoted by τ. The rate at which equilibrium is established within the spin system may, similarly, be characterized by the spin-spin relaxation time, τ'.

There may be quite appreciable differences in the mechanisms of spin-lattice relaxation from one substance to another. Therefore, in addition to being strongly dependent on the temperature of a paramagnetic substance, the magnitude of τ varies over wide limits from one substance to another. In contrast with time τ, the magnitude of τ' depends very

little on lattice temperature. Another difference to be noted between spin-spin and spin-lattice relaxation is that the process of establishing equilibrium with a spin system consists in an exchange of energy between its various parts, although the total energy of the system is conserved; spin-lattice relaxation, however, is associated with a change in the energy of the spin system.

It is clear that the very possibility of dividing a paramagnetic substance into a spin system and a lattice presupposes that the interactions within the spin system (spin-spin interactions) are much stronger than the interactions of the spin system with the lattice (spin-lattice interactions), that is $\tau' << \tau$.

V.1 SPIN-LATTICE RELAXATION

There are basically two ways of approaching the spin-lattice relaxation phenomena. One is to consider the transition probabilities between populated energy levels and to obtain the so-called rate equations, and the other is to follow the phenomenological treatment of Bloch.

THE RATE EQUATIONS

For simplicity, let us consider a two energy level spin system (e.g. $S = 1/2$) E_1 and E_2 ($E_1 < E_2$) with populations n_1 and n_2, respectively. A radiation of frequency $\omega = (E_2 - E_1)/\hbar$ incident upon this system will cause transitions between the two levels in either direction, the number of spins leaving the lower state being proportional to n_1 and the number leaving the upper state being proportional to n_2. Thus, the populations of the two levels obey the differential equation

$$-\frac{dn_1}{dt} = \frac{dn_2}{dt} = w_{12}n_1 - w_{21}n_2 \qquad (5.2)$$

where w_{12} and w_{21} are the rates at which spins make transition from the

lower to the upper state and vice versa. Once a thermal equilibrium is established between the spin system and the incident radiation the populations will no longer change and consequently the time differentials vanish. Thus

$$0 = w_{12}N_1 - w_{21}N_2 \tag{5.3}$$

where N_1 and N_2 stand for the equilibrium populations of the lower and upper level, respectively. If T_o is the equilibrium temperature and ρ is the radiation density, then the transition rates can be written as

$$w_{12} = B\rho \tag{5.4}$$

$$w_{21} = A + B\rho = B\rho \exp(\hbar\omega/kT_o) \tag{5.5}$$

where A and B are the Einstein coefficients of spontaneous emission and stimulated emission (or absorption) respectively. Hence from equation (5.3) we have

$$\frac{w_{21}}{w_{12}} = \frac{N_1}{N_2} = \exp(\hbar\omega/kT_o) \tag{5.6}$$

If the spin system is not in thermal equilibrium with the incident radiation, from equation (5.2)

$$\frac{d(n_1 - n_2)}{dt} = -2(w_{12}n_1 - w_{21}n_2)$$

$$= (n_1 + n_2)(w_{21} - w_{12}) - (w_{21} + w_{12})(n_1 - n_2) \tag{5.7}$$

Defining

$$n_1 + n_2 = N$$

$$n_1 - n_2 = n$$

equation (5.7) can be written as

$$\frac{dn}{dt} = N(w_{21} - w_{12}) - n(w_{21} + w_{12})$$

$$= (w_{21} + w_{12}) \left[N \frac{w_{21} - w_{12}}{w_{21} + w_{12}} - n \right]$$

$$= \frac{n_o - n}{T_1} \qquad (5.8)$$

where

$$n_o = N \frac{w_{21} - w_{12}}{w_{21} + w_{12}}$$

and

$$\frac{1}{T_1} = (w_{21} + w_{12}) \qquad (5.9)$$

Since the solution of the equation (5.8) is

$$n = n_o + C \exp(-t/T_1) \qquad (5.10)$$

where C is a constant of integration, it can therefore be noticed that n_o represents the thermal equilibrium population difference and T_1 is a characteristic time associated with the approach to thermal equilibrium. T_1 is called the "spin-lattice relaxation time."

BLOCH EQUATIONS

In his phenomenological theory of paramagnetic resonance, Bloch [47] introduced two relaxation times: the longitudinal T_1 and the transverse T_2. Let the paramagnetic sample be situated in a static magnetic field $\overline{H}_o$. The time T_1 then characterizes the rate at which the equilibrium state is established if there is an instantaneous change in the magnitude of the field $\overline{H}_o$, assuming its direction is preserved. It is a measure of the rate at which the magnetization M_z of the spin system approaches its equilibrium value M_o. The time T_2 determines the relaxation if there is an instantaneous change in the direction of the field $\overline{H}_o$ while its absolute magnitude is preserved. It is the characteristic time in which the individual processing spins get out of phase

with each other and thus it corresponds to the decay rate of the transverse components M_x and M_y of the magnetization.

The time T_1 characterizes the process of establishment of the equilibrium, related to the change in spin system energy, and may therefore be identified with the spin-lattice relaxation time τ. The time T_2 describes the rate of the relaxation process whereby the energy of the spin system remains unchanged; it may be identified with the time τ'. However, the equivalences of the time τ to T_1, and τ' to T_2 will not always hold. This is because the concepts of longitudinal and transverse relaxation times T_1 and T_2 may always be introduced, while the times τ and τ' have meaning only if $\tau >> \tau'$.

If in addition to the field $\bar{H}_o$, an alternating magnetic field $\bar{H}_1$ is applied in the xy plane at right angles, then the paramagnetic spins will tend to process with the Larmor (resonance) frequency $\omega_o = \gamma H_o$. In the absence of saturation effects the magnetization M will obey the equation

$$\frac{d\bar{M}}{dt} = \gamma \bar{M} \times \bar{H}$$

where γ ($= g\beta/\hbar$) is the gyromagnetic ratio and $\bar{H} = \bar{H}_o + \bar{H}_1$. Furthermore, if the relaxation mechanisms are added to this equation, then its three components constitute the well known Bloch equations:

$$\frac{dMx}{dt} = \gamma (\bar{M} \times \bar{H})_x - \frac{Mx}{T_2} \qquad (5.11a)$$

$$\frac{dMy}{dt} = \gamma (\bar{M} \times \bar{H})_y - \frac{My}{T_2} \qquad (5.11b)$$

$$\frac{dMz}{dt} = \gamma (\bar{M} \times \bar{H})_z - \frac{M_z - M_o}{T_1} \qquad (5.11c)$$

The steady state solution of these Bloch equations (i.e. when $dM_z/dt = 0$) in the presence of an oscillating field $2H_1 \exp(i\omega t)$ is well known and, if the complex susceptibility is defined in the usual

way, $\chi = \chi' - i\chi''$, it can easily be obtained:

$$\chi' = \frac{1}{2}\chi_o \omega_o T_2 \frac{T_2 (\omega_o - \omega)}{1 + T_2^2 (\omega_o - \omega)^2 + \gamma H_1^2 T_1 T_2} \tag{5.12a}$$

$$\chi'' = \frac{1}{2}\chi_o \omega_o T_2 \frac{1}{1 + T_2^2 (\omega_o - \omega)^2 + \gamma^2 H_1^2 T_1 T_2} \tag{5.12b}$$

where the static susceptibility $\chi_o = M_o/H_o$. The mean rate of energy absorption, from the radiation field, is given by

$$I = \frac{\omega}{2\pi} \int_o^{2\pi/\omega} \bar{H}_o \cdot \frac{d\bar{M}}{dt} = 2\omega\chi'' H_1^2$$

$$= \frac{\omega \omega_o \chi_o T_2 H_1^2}{1 + T_2^2 (\omega_o - \omega)^2 + \gamma^2 H_1^2 T_1 T_2} \tag{5.13}$$

which defines the usual resonance curve. It can be seen from equation (5.13) that for frequencies near resonance, i.e. $\omega \to \omega_o$, the height of the absonance curve falls as H_1 is increased. This phenomenon is called "saturation" of the spin system and leads to a method of measuring T_1.

It has been shown that Bloch's phenomenological equations are correct if no spin-spin interactions exist and if the paramagnetism is of the pure spin type (no splitting of the spin energy levels by electric fields). Thus, the Bloch phenomenological equations are applicable over a very limited domain. It is rather extensively used, however, since it gives a qualitative explanation of different aspects of paramagnetic resonance phenomena.

Again, it is not proposed to give a detailed account of the several different theories involved in the explanation of the rather difficult subject of spin-lattice relaxation, but merely to mention briefly the nature of the interactions that determine the value of T_1.

In any case there exists a considerable number of treatises and texts which explain 'a profundis' the phenomenon of magnetic relaxation and that should be consulted for further information.

The first discussion of the spin-lattice relaxation mechanisms by Waller [48] was based on modulation of the spin-spin interaction by the phonons, which induces oscillatory components in the distances between paramagnetic ions, but this theory led to relaxation times appreciably longer than those observed experimentally by Gorter[49] among others. A more potent mechanism and one which, unlike that of Waller, is independent of the degree of concentration of the magnetic ions, is modulation of the ligand field by the lattice vibrations. This produces primarily a fluctuating magnetic field, which modulates the orbital motion of the magnetic electrons. There is no direct interaction with the electron spins, but they feel the effect of the modulation of the orbital motion through the spin-orbit coupling, in the same way as they feel the effects of the static ligand field. The resultant spin-lattice relaxation times are therefore greatly dependent on the extent to which the orbital moment is absent in the free ion, or quenched by the static ligand field.

It was Van Vleck [50] who laid the foundations of the quantitative formulation of the theory of spin-lattice relaxation through modulation of the ligand field, and these have been extended by many others, notably Orbach [51]. There are many complications to be considered, but in the majority of cases the temperature dependence of the spin-lattice relaxation time can be written as

$$1/T_1 = AT + BT^n + C \exp(-\Delta/kT)$$

where the various terms arise from different processes that contribute to the relaxation rate and which can be summarized as follows:

(i) Direct process, by which the spins exchange quanta of energy with lattice modes having the same frequency as the spin resonance frequency. The frequencies of the lattice modes are considered distributed according to a Debye spectrum. When a spin relaxes, it emits a quantum of acoustic energy (phonon) within a narrow band of energies, into one of these modes.

(ii) Raman process, a two-phonon process in which all phonons can take part, giving the strongly temperature dependent second term. The spin interacts simultaneously with two lattice modes whose difference frequency is the spin resonance frequency. This is a second order process, and is less probable than the direct process, but the number of different combinations of frequencies satisfying the necessary resonance condition is very large. The probability of Raman-type relaxation increases according to a T^7 or T^9 law, whereas that of the direct process varies only linearly with temperature.

The net result of these two effects is that the former usually dominates in the liquid helium range of temperatures, whilst the latter dominates at higher temperatures.

(iii) Orbach process, which accounts for the third term, involves absorption of a phonon by a direct process to excite the spin system to a much higher level. These spins then relax to the lower level in the ground doublet by emitting a phonon of slightly higher energy. This difference in energies is again lost by the spins, resulting in an effective transition between the two lower levels. This "resonant two-phonon process" is only possible if there is another energy level at $\Delta < k\theta_D$ (θ_D is the Debye temperature) so that phonons are available to cause this transition. This process differs from the Raman process in that the Raman process takes place via a virtual intermediate level, and in that any virtual level will suffice for the Raman process and

consequently many phonons may contribute, whereas the Orbach process uses only a narrow band of phonons at $h\nu = \Delta$. This process is also strongly temperature dependent.

V.2 EXPERIMENTAL RESULTS

As a precursor to measurements at Q-band of spin-lattice relaxation time, T_1, the room temperature spectra at $\theta = 0^o$ were observed at a frequency of 35.5 GHz. These had a form similar to that obtained at X-band (see Fig.4.1), i.e. the five lines showed clearly, although of course the values of resonance magnetic fields were different. Henderson et al[52] have presented the computer-calculated energy levels in the Q-band region for the tetragonal Fe^{3+} system in MgO; however, there appears to be no published calculated energy levels, in the same energy range, for MgO:Fe^{3+} in sites of octahedral symmetry, which is the case under consideration here. Nevertheless, the line positions of Fig.5.1 fit well with linear extrapolations of the levels given in Fig.2.5 and also agree with the Q-band spectrum reported by Cheng and Kemp[53] in a recent publication.

Using the pulse saturation technique, as briefly described in Chapter III, spin-lattice relaxation time measurements for the $\frac{1}{2} \leftrightarrow -\frac{1}{2}$ transition were carried out at liquid helium temperature (4.2 K) with the samples reference numbers 1,2 and 3. In most of the semi-logarithmic plots produced from the photographs of the exponential decay curves, the existence of two relaxation rates could be observed, one much faster than the other; the longest relaxation time was taken as the spin-lattice relaxation time whilst the shortest one was attributed to a fast relaxation mechanism such as cross-relaxation[54]. Accordingly, for the 140, 310 and 710 p.p.m. Fe specimens the measured relaxation times were 1, 0.7 and 0.1 milliseconds, respectively which seem to indicate

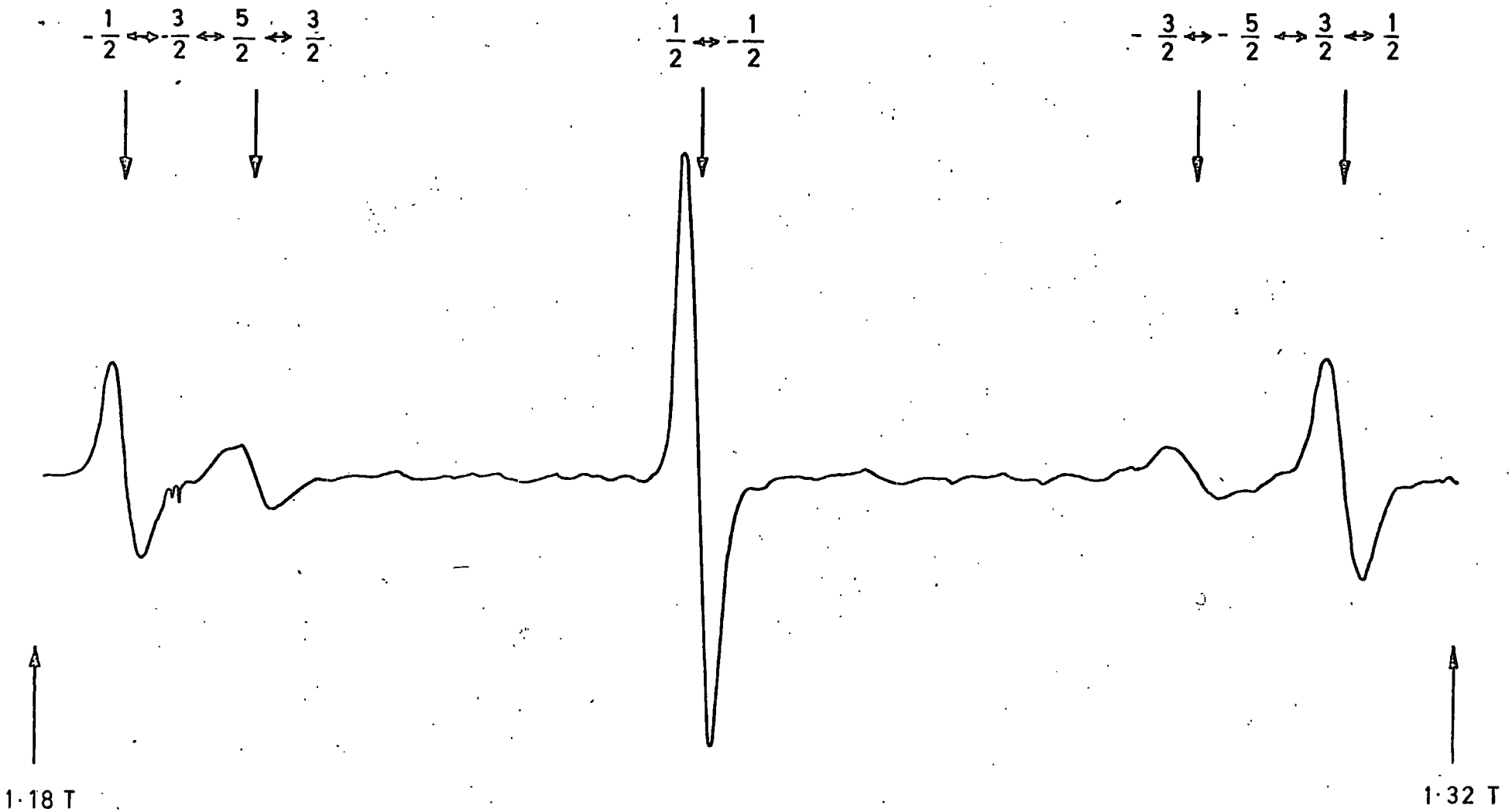

FIG. 5·1 Microwave Spectrum of Iron doped Magnesium Oxide; room temperature, $\theta = 0^{\circ}$, 35·5 GHz, 310 ppm Fe.

that T_1 is somewhat concentration dependent decreasing in magnitude as the concentration increases. The aforementioned values of T_1 were obtained for the d.c. magnetic field oriented along the fourfold axis of the crystal. As Figure 5.2 shows, it is apparent that T_1 behaves in a seemingly periodic manner as the angle of θ between the d.c. field and the <100>-axis varies from $\theta = 0^{\circ}$ to $\theta = 90^{\circ}$. The two minima that could be observed, particularly with the 310 p.p.m. Fe sample (which did not show "extra" lines in the spectrum as the 140 and 710 p.p.m. Fe did), happen to occur, approximately, at angles in which the $-\frac{3}{2} \leftrightarrow -\frac{1}{2}$ and $\frac{1}{2} \leftrightarrow \frac{3}{2}$ transitions are expected to overlap with the main transition. As far as T_1 measurements are concerned, it should be pointed out that it was not possible to obtain data with the rest of the samples (i.e. high Fe concentrations) because the exponential decay could not be observed, even though the oscilloscope registered a very intense d.c. level due to the resonance signal, and, in the light of the observed concentration dependence, it was suggested that T_1 for these samples was too short for the exponential decay to be detected with the aid of the 0.1 μsec/cm-minimum-time-base oscilloscope in use.

In addition to the above mentioned experiments, some T_1-temperature dependence measurements were also performed with the 310 p.p.m. Fe sample. The experimental points which are depicted in Fig. 5.3 appear to be scattered along the T^{-1} and T^{-7} theoretical straight lines which are indicative of direct and Raman regions, respectively.

The data which has been reported so far refers to the samples in the as received state, and some other results were obtained with the heat treated crystals. Relaxation time experiments with the samples reference numbers 1 and 2, after they were baked in air (to increase the ratio Fe^{3+}/Fe^{2+}), showed some striking results: the values of T_1 and its polar variation remained almost the same for the 310 p.p.m. Fe sample

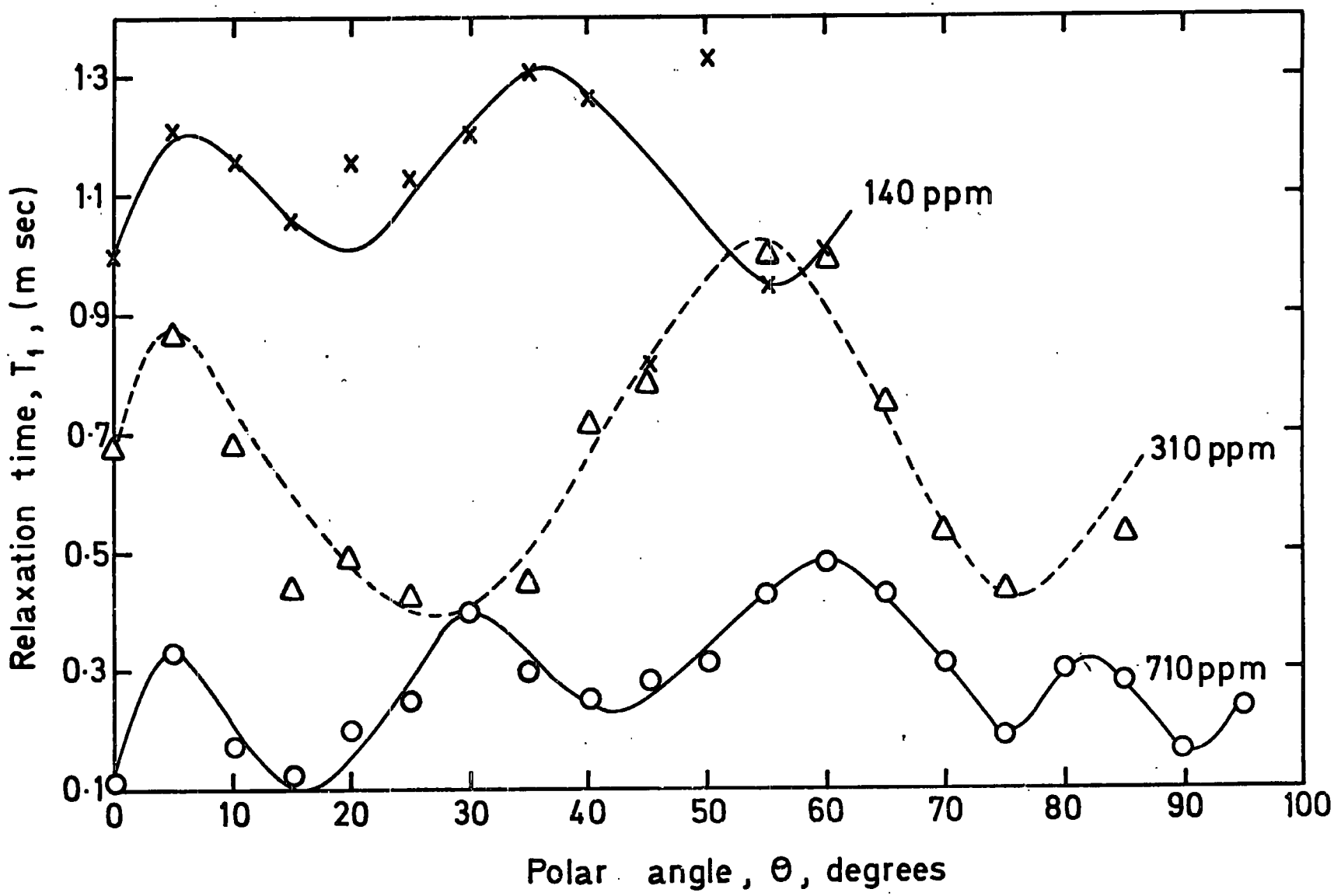

FIG. 5·2. Polar variation of T_1; Fe/MgO, $\frac{1}{2} \leftrightarrow -\frac{1}{2}$ transition, 4·2 K

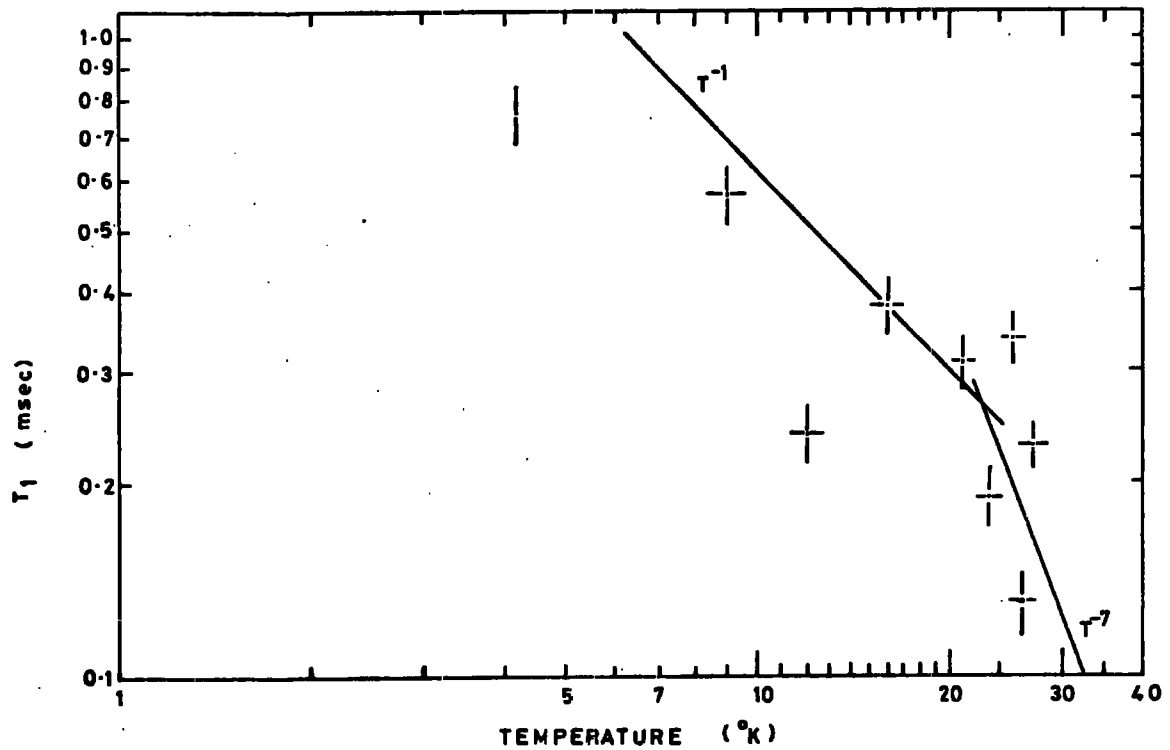

FIG 5·3. Temperature dependence of T_1 ; Fe/MgO, 310ppm Fe.

except for a sudden increase of T_1 ($\sim$ 3 msec) at $\theta = 60^{\circ}$; with the 140 p.p.m. Fe sample a drastic reduction was observed in the absolute value of T_1 ($\sim$ 0.4 msec) and the apparent periodicity observed before the baking process disappeared and instead a 'dip' in the plotted points was observed at $\theta = 60^{\circ}$, T_1 being at this angle about 0.1 msec. No further experiments were possible with the samples after they were heat treated in a hydrogen atmosphere due to an unfortunate failure of the high power pulse klystron.

It is evident that all these data should be regarded as preliminary and, consequently, more experimental work ought to be performed before attempting to assert any conclusion. However, although the information accumulated on spin-lattice relaxation time is scanty, a preliminary analysis of the data will be essayed in the light of the linewidth measurements results, and merely as a guide for forthcoming research in the topic.

V.3 DISCUSSION AND CONCLUSIONS

A first analysis of the experimental data reveals the existence of two relaxation rates for Fe^{3+} in the host lattice MgO; it also indicates concentration and angular dependence of T_1 and shows evidence for the existence of direct and Raman regions in the temperature variation. Moreover, by comparison with published data, there also exists indications that the spin-lattice relaxation time is dependent on the square of the resonance frequency in the way predicted by Mattuck and Strandberg[55].

It has long been suggested that at low temperatures and high concentrations, the relaxation of paramagnetic impurities in crystals may be dominated by cross relaxation to fast relaxing sites (e.g. Fe^{2+} sites) and by faster spin-lattice relaxation processes. In view of

the experimental evidence of two relaxation decay curves, which can be described by the sum of two exponentials as proposed by Manenkov and Milyaev[54] for MgO:Mn^{2+}, it is concluded here that such a fast relaxing process takes place for MgO:Fe^{3+} and it is explained on the basis of spin exchange-interactions (Fe^{3+} - Fe^{3+}) even at low levels of concentration (140 p.p.m. Fe), by correlation with the linewidth model proposed in the previous chapter. For Mn^{2+} in MgO, Solomon[56] has found that by heating a crystal in a hydrogen atmosphere the relaxation time increased by a factor of 10 and, since the procedure more than tripled the concentration of Fe^{2+} ions, he concluded that cross relaxation to the rapidly relaxing Fe^{2+} spins (which should become faster as the Fe^{2+} concentration increases) is not an important part of the spin-lattice relaxation process. Similarly, it is expected here that Fe^{2+} does not play an important role on the spin-lattice relaxation process of MgO:Fe^{3+} but, unlike Solomon, not on experimental grounds but taking into account the linewidth information.

As the energy levels of MgO:Fe^{3+} are not uniformly spaced, rapid transfer of energy to all parts of the system is impeded and different parts of the spin system may have different temperatures; therefore it is possible to observe cross-relaxation between different parts of the spin system. This argument may be used to explain the angular dependence of T_1 (e.g. for the 310 p.p.m. Fe sample). There exists cross-relaxation between the main transition and the "satellites" and, consequently, the spin-lattice relaxation time becomes shorter as the satellites move towards the $\frac{1}{2} \leftrightarrow -\frac{1}{2}$ transition. This cross-relaxation may also account for the concentration dependence of T_1 since a general feature of the cross relaxation phenomena is the increase of the cross-relaxation rate (i.e. shorter T_1) as a function of concentration. One way of evaluating the intrinsic concentration dependence of T_1 is to

measure the longest T_1 for a given ion concentration, and assume this value to be an upper limit. Solomon[56] has applied this idea to the case of MgO:Mn^{2+} and found that T_1 is roughly proportional to the inverse of concentration. In the present case, by analogy, adopting T_1 = 1 msec (140 p.p.m. Fe) as the upper limit yields a proportionality constant A = 140 for a $(\text{concentration})^{-1}$ law; this figure in turn can be used to predict the values of T_1 for the 310 and 710 p.p.m. Fe samples. These predicted values, together with the experimental ones are listed below:

Fe concent. (p.p.m.)	Predicted T_1 (msec)	Exper. T_1 (msec)
310	0.5	0.7
710	0.2	0.1

Since there is a close agreement between the two sets of values, it is very tempting to conclude that for MgO:Fe^{3+} the spin-lattice relaxation time obeys a $(\text{concentration})^{-1}$ law.

From the theory of Mattuck and Strandberg[55] it is predicted that the relaxation time varies inversely with the square of the resonance frequency. Because the measurements reported here were made at a fixed frequency of 35.5 GHz, they provide by themselves no information on the frequency dependence of the relaxation time; however, Castle and Feldman[54] have measured relaxation times at 9.0 GHz which agreed with the values computed by Shiren[58] via measurements of spin-phonon (G_{11},G_{44}) coupling constants. Using these 9 GHz results*, and

* From Shiren's paper three values of T_1 can be worked out for the $\frac{1}{2} \leftrightarrow -\frac{1}{2}$ transition, as expected[59] for ions with S = 5/2; at 4.2 K these are 50, 25.2 and 7.62 msec. From these, T_1 = 25.2 msec has been adopted for the calculation of the constant B since it is in closest agreement with one of Castle and Feldman's experimental values (714 and 23.8 msec) and because it is the most dominant value, as was inferred from Andrew and Tunstall's paper.

assuming $T_1 = B/\nu^2$ (where ν is the resonance frequency), it can be found that the constant of proportionality is $B = 1.92 \times 10^{21}$ which, used to predict a 35.5 GHz spin-lattice relaxation time, yields a value of $T_1 = 1.5$ msec in fairly good agreement with the values measured here. It is, again, tempting to conclude that the $(\text{frequency})^{-2}$ dependence holds for $MgO:Fe^{3+}$.

There is approximate agreement of the experimental points with T^{-1} (direct) and T^{-7} (Raman) lines for the temperature variation which suggests that the slower relaxation process proceeds as for a single ion relaxing to the lattice.

APPENDIX

TABLE 1: Taking 8 unit cells of MgO, the magnesium sites are indexed.

a	b	c	r(Å)	θ°	φ°	a	b	c	r(Å)	θ°	φ°
½	½	0	2.9778	90	45	½	-1	½	5.158	65.91	296.56
-½	½	0	2.9778	90	135	-½	-1	-½	5.158	114.09	243.44
-½	-½	0	2.9778	90	225	½	-1	-½	5.158	114.09	296.56
½	-½	0	2.9778	90	315	1	½	½	5.158	65.91	26.57
0	½	½	2.9778	45	90	1	-½	½	5.158	65.91	333.43
0	-½	½	2.9778	45	270	1	½	-½	5.158	114.09	26.57
0	½	-½	2.9778	135	90	1	-½	-½	5.158	114.09	333.43
0	-½	-½	2.9778	135	270	-1	½	½	5.158	65.91	153.43
½	0	½	2.9778	45	0	-1	-½	½	5.158	65.91	206.56
-½	0	½	2.9778	45	180	-1	½	-½	5.158	114.09	153.43
½	0	-½	2.9778	135	0	-1	-½	-½	5.158	114.09	206.56
-½	0	-½	2.9778	135	180						
						1	0	1	5.956	45	0
0	0	1	4.2112	0	-	-1	0	1	5.956	45	180
0	0	-1	4.2112	180	-	1	0	-1	5.956	135	0
1	0	0	4.2112	90	0	-1	0	-1	5.956	135	180
0	1	0	4.2112	90	90	0	1	1	5.956	45	90
-1	0	0	4.2112	90	180	0	-1	1	5.956	45	270
0	-1	0	4.2112	90	270	0	1	-1	5.956	135	90
						0	-1	-1	5.956	135	270
½	½	1	5.158	35.26	45	1	1	0	5.956	90	45
-½	½	1	5.158	35.26	135	-1	1	0	5.956	90	135
-½	-½	1	5.158	35.26	225	-1	-1	0	5.956	90	225
½	-½	1	5.158	35.26	315	1	-1	0	5.956	90	315
½	½	-1	5.158	144.74	45						
-½	½	-1	5.158	144.74	135	1	1	1	7.294	54.74	45
-½	-½	-1	5.158	144.74	225	-1	1	1	7.294	54.74	135
½	-½	-1	5.158	144.74	315	-1	-1	1	7.294	54.74	225
½	1	½	5.158	65.91	63.44	1	-1	1	7.294	54.74	315
-½	1	½	5.158	65.91	116.56	1	1	-1	7.294	125.26	45
½	1	-½	5.158	114.09	63.44	-1	1	-1	7.294	125.26	135
-½	1	-½	5.158	114.09	116.56	-1	-1	-1	7.294	125.26	225
-½	-1	½	5.158	65.91	243.44	1	-1	-1	7.294	125.26	315

r(Å)	θ_K^o	ϕ_K^o	N (No. of sites)	$Y_{4,0}(\theta_K,\phi_K)$	$Y_{4,4}(\theta_K,\phi_K)$	$Nr^{-6} \times 10^{45} cm^{-6}$	$Nr^{-6} Y_{4,0}(\theta_K,\phi_K)$ $\times 10^{45} cm^{-6}$	$Nr^{-6} Y_{4,4}(\theta_K,\phi_K)$ $\times 10^{45} cm^{-6}$
2.978	90	45	4	0.3174	-0.4425	5.737	1.8209	-2.5386
2.978	45	0	8	-0.3438	0.1106	11.4741	-3.9448	1.2690
4.211	0	-	2	0.8463	0.0000	0.3586	0.3035	0.0000
4.211	90	0	4	0.3174	0.4425	0.7171	0.2276	0.3173
5.158	35.26	45	8	-0.1528	-0.04917	0.4297	-0.06494	-0.02113
5.158	65.91	26.57	16	-0.1087	-0.0861	0.8594	-0.0934	-0.0740
5.956	45	0	8	-0.3438	0.1106	0.1793	-0.0616	0.0198
5.956	90	45	4	0.3174	-0.4425	0.0897	0.0285	-0.0397
7.294	54.74	45	8	-0.3291	-0.1967	0.05313	-0.0175	-0.0105
					SUM	19.898	-1.8017	-1.0823

TABLE 2: Trigonometrical parameters for the magnesium sites in 8 unit cells of MgO .

REFERENCES

1. G. Brown, C.J. Kirkby and J.S. Thorp, J. Mat. Sc. 9, 65 (1974)
2. A. Kelly and G.W. Groves, "Crystallography and Crystal Defects," Longman Group Ltd., London, 1970
3. R.W.G. Wyckoff, "Crystal Structures," Vol.I, Interscience Publishers, N.Y., 1965
4. J.E. Wertz and P. Auzins, Phys. Rev. 106, 484 (1957)
5. H. Bethe, Ann. Physik 3, 133 (1929)
6. J.H. Van Vleck and W.G. Penney, Phil. Mag. 17, 961 (1934)
7. W. Low, Ann. N.Y. Ac. Sc. 72, 69 (1958)
8. W. Low, Phys. Rev. 105, 792 (1957)
9. C.P. Poole and H.A. Farach, "The Theory of Magnetic Resonance," Wiley Interscience, N.Y., 1972
10. S.A. Al'tshuler and B.M. Kozyrev, "Electron Paramagnetic Resonance", Academic Press, N.Y., 1964 (translated by C.P. Poole)
11. W. Low, Phys. Rev. 105, 793 (1957)
12. J.E. Wertz, J.W. Orton and P. Auzins, J. App. Phys. 33, 322 (1962)
13. J.H.E. Griffiths and J.W. Orton, Proc. Phys. Soc. 73, 948 (1959)
14. W. Low, Proc. Phys. Soc. 869, 1169 (1956)
15. P. Debye, Ann. Physik 32, 85 (1938)
16. R. de L. Kronig and C.J. Bouwkamp, Physica 6, 290 (1939)
17. A. Abragam and B. Bleaney, "E.P.R. of Transition Ions," Clarendon Press, Oxford, 1970
18. R.A. Vasquez, "Construccion de un Espectrometro de R.P. a 100 MHz," B.Sc. Thesis, National University of Engineering, Lima, Peru, 1973 (unpublished)
19. C.P. Poole, "Electron Spin Resonance," Interscience Publishers N.Y. 1967
20. G. Brown, D.R. Mason and J.S. Thorp, J. Sci. Inst. 42, 648 (1965)

21. G.A. Woonton, Advan. Electron. Electron Phys. 15, 163 (1961)

22. J.H. Pace, D.F. Sampson and J.S. Thorp, Proc. Phys. Soc. 76 687 (1960)

23. C.F. Davis, M.W.P. Strandberg and R.L. Kyhl, Phys. Rev. 111, 1268 (1958)

24. D.H. Parkinson and J.E. Quarrington, Brit. J. App. Phys. 5, 219 (1954)

25. A.M. Portis, Phys. Rev. 91, 1071 (1953)

26. P.W. Anderson, Phys. Rev. 114, 1002 (1959)

27. J.M. Luttinger and L. Tisza, Phys. Rev. 70, 954 (1946)

28. J.H. Van Vleck, Phys. Rev. 74, 1168 (1948)

29. J.H. Van Vleck, Nuovo Cimento Suppl. 6, 993 (1957)

30. J.D. Jackson, "Classical Electrodynamics," Wiley, N.Y., 1962

31. J. Toussaint and C. Declerek, Bull. Soc. Roy. Sci. Liege 1, 93 (1966)

32. J.B. Jones and M.F. Lewis, Solid St. Comm. 5, 595 (1967)

33. M.F. Lewis, Solid St. Comm. 5, 845 (1967)

34. J.E. Wertz, G. Saville, P. Auzins and J.W. Orton, J. Phys. Soc. Japan 18, Suppl. II. 305 (1963)

35. W. Low and M. Weger, Phys. Rev. 118, 1130 (1960)

36. W.J.C. Grant and M.W.P. Strandberg, Phys. Rev. 135A, 727 (1964)

37. J.S. Thorp and H.P. Buckley, J. Mat. Sc. 9, 1499 (1974)

38. C.J. Gorter and J.H. Van Vleck, Phys. Rev. 72, 1128 (1947)

39. N. Bloembergen, E.M. Purcell and R.V. Pound, Phys. Rev. 73, 679 (1948)

40. G.D. Jones, Phys. Rev. 155A, 259 (1967)

41. F.A. Cotton and M.D. Meyers, J. Am. Chem. Soc. 82, 5023 (1960)

42. R.D. King and B. Henderson, Proc. British Ceram. Soc. 9, 63 (1967)

43. Y.K. Zavoisky, Sov. Fiz. 10, 197 (1946). Mentioned in reference 10, pp.10.

44. A.M. Stoneham, K.A. Müller and W. Berlinger, Solid St. Comm. 10, 1005 (1972)

45. C.J. Gorter, "Paramagnetic Relaxation", Elsevier Publishing Co. Amsterdam, 1947

46. H.B.G. Casimir and F.K. du Pre, Physica 5, 507 (1938)

47. F. Bloch, Phys. Rev. 70, 460 (1946)

48. I. Waller, Z. Phys. 79, 370 (1932)

49. C.J. Gorter, Physica 3, 503 (1936)

50. J.H. Van Vleck, Phys. Rev. 57, 426 (1940)

51. R. Orbach, Proc. R. Soc. A264, 458, 485 (1961)

52. B. Henderson, J.E. Wertz and P.P. Halls, J. Phys. C. (Solid St. Phys.) 4, 107 (1971)

53. J.C. Cheng and J.C. Kemp, Phys. Rev. B4, 2841 (1971)

54. A.A. Manenkov and V.A. Milyaev, "Paramagnetic Resonance" (Proceedings of the First International Conference held in Jerusalem, July 1962) edited by W. Low, Ac. Press, N.Y. 1963

55. R.D. Mattuck and M.W.P. Strandberg, Phys. Rev. 119, 1204 (1960)

56. P.R. Solomon, Phys. Rev. 152, 452 (1966)

57. J.G, Castle and D.W. Feldman, mentioned in ref. 58

58. N.S. Shiren, Proc. XIth Colloque Ampere, 1962, pp.114

59. E.R. Andrews and D.P. Tunstall, Proc. Phys. Soc. 78, 1 (1961)